

A generalised algorithm for anelastic processes in elastoplasticity and biomechanics

Original

A generalised algorithm for anelastic processes in elastoplasticity and biomechanics / Grillo, Alfio; Prohl, Raphael; Wittum, Gabriel. - In: MATHEMATICS AND MECHANICS OF SOLIDS. - ISSN 1081-2865. - 22:3(2017), pp. 502-527. [10.1177/1081286515598661]

Availability:

This version is available at: 11583/2627605 since: 2020-06-02T09:26:20Z

Publisher:

SAGE Publications

Published

DOI:10.1177/1081286515598661

Terms of use:

This article is made available under terms and conditions as specified in the corresponding bibliographic description in the repository

Publisher copyright

Sage postprint/Author's Accepted Manuscript

Grillo, Alfio; Prohl, Raphael; Wittum, Gabriel, A generalised algorithm for anelastic processes in elastoplasticity and biomechanics, accepted for publication in MATHEMATICS AND MECHANICS OF SOLIDS (22 3) pp. 502-527. © 2017 (Copyright Holder). DOI:10.1177/1081286515598661

(Article begins on next page)

A Generalised Algorithm for Anelastic Processes in Elastoplasticity and Biomechanics*

Alfio Grillo[†], Raphael Prohl[‡], Gabriel Wittum[§]

DOI: <https://doi.org/10.1177/1081286515598661>. Available online: September 15, 2015

Journal: *Mathematics and Mechanics of Solids* (SAGE)

Abstract

A computational algorithm for solving anelastic problems in finite deformations is introduced. The presented procedure, termed Generalised Plasticity Algorithm (GPA) hereafter, takes inspiration from the Return Mapping Algorithm (RMA), which is typically employed to solve the Karush-Kuhn-Tucker (KKT) system arising in finite Elastoplasticity, but aims to modify and extend the RMA to the case of more general flow rules and strain energy density functions as well as to non-classical formulations of Elastoplasticity, in which the plastic variables are not treated as internal variables. To assess its reliability, the GPA is tested in two different contexts. Firstly, it is used for solving two classical problems (a shear-compression test and the necking of a circular bar). In both cases, the GPA is compared to the RMA in terms of structural set-up, computational effort and flexibility, and its convergence is evaluated by solving several benchmarks. Some restrictions of the classical form of the RMA are pointed out, and it is shown how these can be overcome by adopting the proposed algorithm. Secondly, the GPA is applied to characterise the mechanical response of a biological tissue that undergoes large deformations and remodelling of its internal structure.

Keywords: Finite Strain Elastoplasticity, Return Mapping Algorithm, Generalised Plasticity Algorithm.

1 Introduction

Anelastic processes constitute a widely investigated research subject of both theoretical and computational Mechanics. They play an important role in the characterisation of the mechanical response of continuum bodies that undergo reorganisations of their internal structure, besides deforming under the action of applied stimuli.

The interest in the evolution of the internal structure of continuum bodies ranges over various physical contexts, including industrial and biomechanical problems. In the case of industrial applications, a confident description of the elastoplastic behaviour of building materials, such as metals, is necessary to characterise their mechanical properties under

*Dedicated to Prof. R. A. Toupin, in recognition of his contributions to science.

[†]Corresponding Author. DISMA “G. L. Lagrange”, Politecnico di Torino. Corso Duca degli Abruzzi 24, I-10129, Torino (TO), Italy. Tel.: +39 011 090 7531. Fax: +39 011 090 7599. E-mail: alfio.grillo@polito.it

[‡]Steinbeis Center, Simulation in Technology, Bussardweg 6, D-75446 Wiernsheim, Germany. E-mail: raphael@techsim.org

[§]G-CSC, Goethe Universität Frankfurt. Kettenhofweg 139, D-60325, Frankfurt am Main, Germany. E-mail: wittum@gcsc.uni-frankfurt.de

33 severe working conditions. In Biomechanics, the mathematical description of anelastic
34 processes is required, for instance, to study the growth and remodelling (structural adap-
35 tation) of biological tissues. These phenomena are of great importance in the evolution
36 and differentiation of tissues both in physiological and pathological situations, and apply
37 to bone, articular cartilage, blood vessels and tumours. In all these cases, efficient and
38 robust numerical methods have to be supplied to simulate reliably the material response.

39 Although the physics behind the onset of anelastic distortions in industrial materials
40 is very different from that inherent in biological tissues, the mathematical models and
41 the computational strategies addressing anelastic problems share many common features,
42 and take inspiration from the Theory of Elastoplasticity, a rich research theme to which
43 many authors have contributed (cf., e.g., [1, 2] and the references therein), and in which
44 many efforts have been put for developing numerical methods (cf., e.g., [3, 4, 5, 6, 7, 8, 9]).
45 In addition, reference should be made to the fundamental theories of Toupin [10] and
46 Mindlin [11, 12].

47 To the best of the authors' knowledge and understanding, the crucial differences among
48 the various models of Elastoplasticity arise when the issues of plastic flow and hardening
49 are addressed. Taking for granted the Bilby-Kröner-Lee (BKL) multiplicative decomposi-
50 tion of the deformation gradient into an elastic and a plastic part, and describing hardening
51 through a suitable hardening variable (in general, a second-order tensor field), the classical
52 models of Elastoplasticity often treat the tensor of plastic distortions and the hardening
53 variable as internal variables (cf., e.g., [13, 14, 15]). This is, however, not always the case.
54 Indeed, both in Elastoplasticity and in the Biomechanics of tissue remodelling, there exist
55 theories in which the tensor of plastic distortions is viewed as a kinematic entity that,
56 together with the standard motion, determines the kinematics of a body [16, 17]. Another
57 aspect, in which models of Plasticity differ from each other, is the formulation of the flow
58 rule. Many models assume associative flow rules, which means that the plastic strain rate
59 is derivable from the function defining the yield surface of the considered material [1]. In
60 other circumstances, instead, non-associative flow rules must be considered (cf., e.g., [18]).

61 In Biomechanics, the BKL decomposition was introduced by Rodriguez *et al.* [19],
62 who associated the processes of growth and remodelling with the occurrence of anelastic
63 distortions. In [20], the anelastic distortions accompanying growth were interpreted as
64 “local rearrangement of material inhomogeneities”, and their evolution was shown to be
65 driven by the Mandel stress tensor. In the theories of tumour growth [21] and remodelling
66 of cellular aggregates [22], the “evolving natural configurations” [23] were exploited to
67 define the anelastic distortions related with these processes.

68 A common computational method used to solve elastoplastic problems is the Return
69 Mapping Algorithm (RMA). In its classical form, the RMA is a closest point projection
70 method, presented under the hypotheses of associative flow rule and isotropic elastoplastic
71 material behaviour [15]. The elastoplastic problem is reduced to a constrained optimisation
72 problem, subjected to a set of Karush-Kuhn-Tucker (KKT-) conditions. Other algorithms
73 have their origin in optimisation theory, like, e.g., the methods of Sequential Quadratic
74 Programming (SQP) [24].

75 This manuscript sets itself two scopes. The first one is to present an algorithm that,
76 on the one hand, can be applied to complex, non-linear anelastic problems (such as those
77 involving the derivatives of plastic distortions) and that, on the other hand, may serve
78 as a basis for developing an efficient solver for Structural Mechanics. Since it has been
79 conceived as a generalisation of the classical RMA, and it has been applied for solving
80 both elastoplastic problems of industrial interest and biomechanical problems of tissue
81 remodelling, the proposed procedure has been named Generalised Plasticity Algorithm

82 (GPA). The GPA accounts for geometric and kinematic non-linearities, as well as for the
 83 non-linear constitutive behaviour of the considered materials.

84 The GPA is formulated in two contexts. In the first one, it aims to be an alternative to
 85 the classical RMA for elastoplastic models that fail to comply with all the hypotheses on
 86 which the standard RMA is based. To encompass more general flow rules, and to account
 87 for the cases in which the flow rules cannot be decoupled from the weak form of the
 88 momentum balance law, the GPA requires a linearisation with respect to the deformation
 89 and one with respect to the tensor of anelastic distortions. This means that, compared
 90 with the classical RMA, an additional linearisation iteration is performed in the GPA. In
 91 contrast to the SQP method, the GPA is not found by formulating a sequence of quadratic
 92 subproblems. Rather, the KKT-system is linearised with respect to the deformation and
 93 the tensor of anelastic distortions in the full non-linear elastoplastic regime.

94 The second scope of this work is to highlight the connection between mathematical
 95 modelling and numerics. Indeed, the GPA, which is inspired by the theories developed
 96 in [16, 17], stems from the fact that a model in which the standard motion and the
 97 anelastic distortions are viewed as equally ranked kinematic descriptors (rather than as
 98 a kinematic descriptor and an internal tensor variable) naturally requires a reformulation
 99 of the Principle of Virtual Powers. This, in turn, leads to the necessity of adapting the
 100 already well-established numerical methods of inelastic processes to more general solution
 101 strategies, thereby including novel discretisation schemes and linearisation algorithms.

102 Although the computational effort required by the GPA is higher than that of the
 103 RMA, the GPA seems to be more versatile and applicable to a wider variety of flow rules,
 104 elastoplastic behaviours, formulations of Elastoplasticity, and biomechanical problems.

105 The paper is organised as follows. Section 2 summarises the theoretical basis of the
 106 work. In section 3, all constitutive assumptions are reviewed in detail. In section 4, the two
 107 types of problems addressed in the paper, referred to as ‘Pr1’ and ‘Pr2’, are formalised.
 108 Section 5 is dedicated to review the RMA, while the proposed algorithm, the GPA, is
 109 presented in section 6. The problem ‘Pr1’ encompasses the von Mises J_2 theory of isochoric
 110 and associative plasticity, and is solved by applying both the standard RMA and the
 111 GPA in order to evaluate the functionality of the latter algorithm. The problem ‘Pr2’ is
 112 formulated in a more general framework, and its applicability to the biomechanical context
 113 is evidenced. The numerical results are shown in section 7, where the differences between
 114 the GPA and the RMA are discussed in detail. The philosophy of the work and some ideas
 115 for future research are discussed in section 8.

116 2 Theoretical Background

117 The formalism adopted hereafter follows [25], with some modifications. In the following,
 118 \mathcal{B} is the three-dimensional manifold describing a solid body, \mathcal{S} is the three-dimensional
 119 Euclidean space and $J \subseteq \mathbb{R}$ is the interval of time over which the evolution of the body is
 120 observed. A motion is the one-parameter family of smooth mappings $\chi(\cdot, t) : \mathcal{B} \rightarrow \mathcal{S}$, with
 121 $t \in J$. The set $\mathcal{C}_t = \chi(\mathcal{B}, t) \subset \mathcal{S}$ is referred to as current configuration. For every $X \in \mathcal{B}$
 122 and $t \in J$, there exists a spatial point $x \in \mathcal{C}_t$ such that $x = \chi(X, t)$. In the following, \mathcal{S} is
 123 assumed to be equipped with the structure of affine space.

124 Given the space of free vectors \mathcal{V} , obtained by translating the points of \mathcal{S} , the space
 125 $T_x\mathcal{S} = \{\mathbf{v}_x \in \mathcal{V} \mid \mathbf{v}_x = y - x, y \in \mathcal{S}\}$ is the tangent space of \mathcal{S} at x . Its dual space $T_x^*\mathcal{S}$ is
 126 the cotangent space at x . The disjoint unions $T\mathcal{S} = \sqcup_{x \in \mathcal{S}} T_x\mathcal{S}$ and $T^*\mathcal{S} = \sqcup_{x \in \mathcal{S}} T_x^*\mathcal{S}$ are the
 127 tangent bundle and cotangent bundle, respectively. With analogous notation, $T_X\mathcal{B}$ denotes
 128 the tangent space of \mathcal{B} at X , and its dual space, $T_X^*\mathcal{B}$, is the cotangent space at X . Then,

129 $T\mathcal{B} = \sqcup_{X \in \mathcal{B}} T_X \mathcal{B}$ and $T^*\mathcal{B} = \sqcup_{X \in \mathcal{B}} T_X^* \mathcal{B}$ are the tangent bundle and the cotangent bundle
130 of \mathcal{B} , respectively.

131 The velocity of a material particle passing through $x = \chi(X, t)$ at time t is denoted
132 by $\mathbf{v}(x, t) \in T_x \mathcal{S}$. It holds that $\mathbf{v}(x, t) = \mathbf{u}(X, t) = \dot{\chi}(X, t)$, where the superimposed dot
133 stands for partial differentiation with respect to time, and $\mathbf{u}(\cdot, t) : \mathcal{B} \rightarrow T\mathcal{S}$ is defined by
134 $\mathbf{u}(X, t) = \mathbf{v}(\chi(X, t), t)$. The tangent map of $\chi(\cdot, t)$ at X , with $t \in \mathcal{J}$, is the deformation
135 gradient tensor $T\chi(X, t) = \mathbf{F}(X, t) : T_X \mathcal{B} \rightarrow T_{\chi(X, t)} \mathcal{S}$, with $J := \det(\mathbf{F}) > 0$ for all $t \in \mathcal{J}$
136 and for all $X \in \mathcal{B}$.

137 Given the metric tensor $\mathbf{g} : T\mathcal{S} \rightarrow T^*\mathcal{S}$, the pull-back of \mathbf{g} through χ is the right Cauchy-
138 Green deformation tensor $\mathbf{C} = \mathbf{F}^T \cdot \mathbf{F} = \mathbf{F}^T \mathbf{g} \mathbf{F} : T\mathcal{B} \rightarrow T^*\mathcal{B}$, with $\mathbf{F}^T : T^*\mathcal{S} \rightarrow T^*\mathcal{B}$. The
139 tensor $\mathbf{G} : T\mathcal{B} \rightarrow T^*\mathcal{B}$ is the material metric tensor.

140 The second-order tensor field $\boldsymbol{\ell}(\cdot, t) : \mathcal{B} \rightarrow T\mathcal{S} \otimes T^*\mathcal{S}$ is the velocity gradient expressed
141 in terms of the points of \mathcal{B} , i.e. $\boldsymbol{\ell}(X, t) = \text{grad} \mathbf{v}(x, t)$, with $x = \chi(X, t)$. It is related to the
142 material velocity gradient, $\text{Grad} \mathbf{u} = \dot{\mathbf{F}}$, through $\boldsymbol{\ell} = \dot{\mathbf{F}} \mathbf{F}^{-1}$. It holds that $\dot{\mathbf{C}} = \mathbf{F}^T 2\mathbf{d} \mathbf{F}$,
143 where $\mathbf{d} = \text{sym}(\boldsymbol{\ell}^\flat)$ denotes the symmetric part of $\boldsymbol{\ell}^\flat = \mathbf{g} \boldsymbol{\ell} : T\mathcal{S} \rightarrow T^*\mathcal{S}$.

144 Sometimes the kinematics of a continuum body is formulated in terms of one chosen
145 reference configuration rather than in terms of \mathcal{B} . Some words of caution on possible abuses
146 of the concept of ‘reference configuration’ are given in [17, 20, 26].

147 2.1 Bilby-Kröner-Lee Decomposition of the Deformation Gradient

148 One of the theoretical pillars of finite Elastoplasticity is the multiplicative decomposition
149 of \mathbf{F} into an elastic and a plastic part [27]:

$$\mathbf{F} = \mathbf{F}_e \mathbf{F}_p. \quad (1)$$

150 In (1), \mathbf{F} accounts for the global change of shape of the body, \mathbf{F}_p describes the total
151 plastic distortions responsible for the evolution of the body’s internal structure, and \mathbf{F}_e
152 represents the total elastic distortion (in Kröner’s terminology [27], a ‘distortion’ is the
153 superposition of deformation and rotation). A thorough explanation of the physics be-
154 hind (1) can be found, e.g., in [2]. The tensor field $\mathbf{F}_p(\cdot, t)$ transforms the body elements
155 of \mathcal{B} into a collection \mathcal{K}_t of stress-free body elements, which is referred as ‘body’s natural
156 state’. The whole elastic distortion, \mathbf{F}_e , is the distortion that has to be applied to the
157 elements of \mathcal{K}_t to get the global configuration \mathcal{C}_t . Since the body elements collected in the
158 conglomerate \mathcal{K}_t may become geometrically incompatible, \mathcal{K}_t does not generally form a
159 configuration in the Euclidean space. However, a continuous stress-free configuration can
160 be reconstructed in some suitably defined non-Euclidean space [2, 27], whose curvature is
161 induced by incompatibility. The body’s natural state is not unique, since it is defined up
162 to an orthogonal transformation [17, 28].

163 If (1) is viewed as the composition of tangent bundle maps [29], it is possible to in-
164 troduce the mapping $\chi_\kappa(\cdot, t) : \mathcal{B} \rightarrow \mathcal{S}$ that serves as the base map for the bundle map
165 \mathbf{F}_p . The set $\mathcal{C}_\kappa = \chi_\kappa(\mathcal{B}, t) \subset \mathcal{S}$, which represents the subregion of space \mathcal{S} associated
166 with the body’s natural state, is termed ‘intermediate configuration’. The total plastic
167 distortion can be identified with the map $\mathbf{F}_p(X, t) : T_X \mathcal{B} \rightarrow T_{\chi_\kappa(X, t)} \mathcal{S}$, even though
168 \mathbf{F}_p is not the tangent map to χ_κ . Accordingly, the total elastic distortion is written as
169 $\mathbf{F}_e(X, t) \equiv \mathbf{F}(X, t) \mathbf{F}_p^{-1}(X, t) : T_{\chi_\kappa(X, t)} \mathcal{S} \rightarrow T_{\chi(X, t)} \mathcal{S}$. To complete the physical frame
170 within which \mathbf{F}_p and \mathbf{F}_e are conceived, the concepts of material uniformity and homo-
171 geneity should be discussed [26, 30, 31].

172 Granted the multiplicative decomposition (1), and denoting by $\boldsymbol{\eta}(\xi)$ the metric tensor
173 associated with $T_\xi \mathcal{S}$, where $\xi = \chi_\kappa(X, t)$, one can define $\mathbf{b}_e = \mathbf{F}_e \cdot \mathbf{F}_e^T = \mathbf{F}_e \boldsymbol{\eta}^{-1} \mathbf{F}_e^T$ and

174 $\mathbf{B}_p = \mathbf{F}_p^{-1} \boldsymbol{\eta}^{-1} \mathbf{F}_p^{-T}$. The former is the left Cauchy-Green tensor generated by the elastic
 175 distortions, while the latter is the inverse of $\mathbf{C}_p = \mathbf{F}_p^T \cdot \mathbf{F}_p = \mathbf{F}_p^T \boldsymbol{\eta} \mathbf{F}_p$, i.e. the right Cauchy-
 176 Green tensor induced by the plastic distortions. It holds that $\mathbf{b}_e = \mathbf{F} \mathbf{B}_p \mathbf{F}^T$.

177 The decomposition (1) also implies that the velocity gradient $\boldsymbol{\ell}$ splits additively as

$$\boldsymbol{\ell} = \boldsymbol{\ell}_e + \underbrace{\mathbf{F}_e \mathbf{L}_p \mathbf{F}_e^{-1}}_{:=\boldsymbol{\ell}_p} = \boldsymbol{\ell}_e + \boldsymbol{\ell}_p, \quad (2)$$

178 where $\boldsymbol{\ell}_e = \dot{\mathbf{F}}_e \mathbf{F}_e^{-1}$ and $\mathbf{L}_p = \dot{\mathbf{F}}_p \mathbf{F}_p^{-1}$ denote, respectively, the rates of elastic and plastic
 179 distortions. The rates of \mathbf{b}_e and \mathbf{B}_p are related to each other by means of the expressions

$$\mathcal{L}_v \mathbf{b}_e = \mathbf{F} \overline{[\mathbf{F}^{-1} \mathbf{b}_e \mathbf{F}^{-T}]} \mathbf{F}^T = \mathbf{F} \dot{\mathbf{B}}_p \mathbf{F}^T, \quad (3a)$$

$$\dot{\mathbf{B}}_p = -\mathbf{F}^{-1} \mathbf{F}_e (\boldsymbol{\eta}^{-1} 2 \mathbf{D}_p \boldsymbol{\eta}^{-1}) \mathbf{F}_e^T \mathbf{F}^{-T}, \quad (3b)$$

180 where $\mathcal{L}_v \mathbf{b}_e$ is the Lie derivative of \mathbf{b}_e , while $\mathbf{D}_p = \text{sym}(\boldsymbol{\eta} \mathbf{L}_p)$ is the symmetric part of the
 181 fully covariant tensor $\boldsymbol{\eta} \mathbf{L}_p$.

182 Another consequence of (1) is the decomposition $J = J_e J_p$, where $J_e := \det(\mathbf{F}_e) > 0$
 183 and $J_p := \det(\mathbf{F}_p) > 0$ are the volumetric parts of the elastic and plastic distortions,
 184 respectively. The time derivatives of J_e and J_p are related to the traces of $\boldsymbol{\ell}_e$ and $\boldsymbol{\ell}_p$ by
 185 the expressions $\dot{J}_e = J_e \text{tr}(\boldsymbol{\ell}_e)$ and $\dot{J}_p = J_p \text{tr}(\mathbf{L}_p) = J_p \text{tr}(\boldsymbol{\ell}_p)$. Furthermore, by defining the
 186 deformation gradient tensor as $\mathbf{F} = J^{1/3} \overline{\mathbf{F}}$ [32, 33], an expression is obtained in which
 187 $J^{1/3} \mathbf{i}$ and $\overline{\mathbf{F}}$ represent, respectively, the purely volumetric contribution and the volume-
 188 preserving part of the overall deformation (here, $\mathbf{i} : TS \rightarrow TS$ is the identity tensor in TS).
 189 Thus, from (1) and the identity $J = J_e J_p$, it follows that $\overline{\mathbf{F}} = \overline{\mathbf{F}}_e \overline{\mathbf{F}}_p$.

190 A usual assumption both in metal plasticity and in the biomechanics of remodelling of
 191 biological tissues is that plastic distortions are isochoric, i.e. they must comply with the
 192 constraint $J_p = 1$. This requirement places the restriction

$$\dot{J}_p = -\frac{1}{2} [\det(\mathbf{B}_p)]^{-1/2} \text{tr}(\mathbf{B}_p^{-1} \dot{\mathbf{B}}_p) = 0, \quad (4)$$

193 which means that the time derivative of \mathbf{B}_p is orthogonal to \mathbf{B}_p^{-1} in the sense that their
 194 double contraction vanishes identically, i.e. $\text{tr}(\mathbf{B}_p^{-1} \dot{\mathbf{B}}_p) \equiv \mathbf{B}_p^{-1} : \dot{\mathbf{B}}_p = 0$. When (4) applies,
 195 the relation (3b) becomes

$$\dot{\overline{\mathbf{B}}}_p = -\mathbf{F}^{-1} \mathbf{F}_e (\boldsymbol{\eta}^{-1} 2 \text{dev}(\mathbf{D}_p) \boldsymbol{\eta}^{-1}) \mathbf{F}_e^T \mathbf{F}^{-T}, \quad (5)$$

196 where $\text{dev}(\mathbf{D}_p) = \mathbf{D}_p - \frac{1}{3} \text{tr}(\boldsymbol{\eta}^{-1} \mathbf{D}_p) \boldsymbol{\eta}$ is the deviatoric part of \mathbf{D}_p , and $\overline{\mathbf{B}}_p = \overline{\mathbf{F}}_p^{-1} \cdot \overline{\mathbf{F}}_p^{-T}$
 197 is the volume-preserving part of \mathbf{B}_p . Since the condition $J_p = 1$ is enforced, (5) remains
 198 invariant under the substitution of \mathbf{F} and \mathbf{F}_e with $\overline{\mathbf{F}}$ and $\overline{\mathbf{F}}_e$, respectively.

199 Decompositions of the type (1) were proposed by many authors in problems related
 200 to growth and remodelling of biological tissues, which were studied either as monophasic
 201 continua [20, 21, 34, 35, 36, 37] or as mixtures [38, 39, 40, 41, 42, 43, 44]. A review on
 202 constitutive theories relying on (1) was done in [45].

203 2.2 Principle of Virtual Powers and Dissipation

204 Only a purely mechanical framework is considered hereafter. The body mass is assumed to
 205 be conserved. Thus, if ϱ denotes the spatial mass density of the body, and ϱ_R is its backward
 206 Piola transform (i.e. $\varrho_R(X, t) = J(X, t) \varrho(\chi(X, t), t)$), the mass balance law reduces to
 207 $\dot{\varrho}_R = 0$, which holds at all $X \in \mathcal{B}$ and for all $t \in \mathcal{J}$, i.e. $\varrho_R(X, t) \equiv \varrho_R(X)$ for all times.

208 Within the classical theory of finite Elastoplasticity, the elastoplastic behaviour of a
 209 body is described by its motion, χ , the plastic part of the total deformation, \mathbf{F}_p , and the
 210 hardening variable $\boldsymbol{\alpha}$. In the standard theory, these three types of variables are not treated
 211 in same way, at least conceptually. Indeed, while χ is the solution of the set of equations
 212 governing the body dynamics, \mathbf{F}_p and $\boldsymbol{\alpha}$ are regarded as internal variables determined by
 213 solving evolution laws [13, 15, 46], which are not introduced on the same footing as χ .
 214 In other words, neither \mathbf{F}_p nor $\boldsymbol{\alpha}$ appear explicitly in the formulation of the Principle of
 215 Virtual Powers (PVP), which is established by defining the set of virtual (test) velocities
 216 as the collection of all admissible realisations of the type

$$\tilde{\mathcal{H}} := \{\tilde{\mathbf{u}} : \mathcal{B} \rightarrow T\mathcal{S} \mid \tilde{\mathbf{u}}|_{\partial\mathcal{B}_D} = \mathbf{0}\}. \quad (6)$$

217 In (6), $\partial\mathcal{B}_D$ is the Dirichlet-boundary of \mathcal{B} , i.e. the portion of $\partial\mathcal{B}$ over which position
 218 boundary conditions are enforced, and $\tilde{\mathbf{u}}|_{\partial\mathcal{B}_D}$ is the restriction of $\tilde{\mathbf{u}}$ to $\partial\mathcal{B}_D$.

219 For a first-grade material, the PVP reads

$$\int_{\mathcal{B}} \mathbf{P} : \mathbf{g} \text{Grad } \tilde{\mathbf{u}} = \int_{\mathcal{B}} \mathbf{b}_R \cdot \tilde{\mathbf{u}} + \int_{\partial\mathcal{B}_N} \mathbf{f}_R \cdot \tilde{\mathbf{u}}, \quad \forall \tilde{\mathbf{u}} \in \tilde{\mathcal{H}}, \quad (7)$$

220 and expresses the weak form of the local balance of momentum. In (7), $\mathbf{P} : T^*\mathcal{B} \rightarrow T\mathcal{S}$ is the
 221 first Piola-Kirchhoff stress tensor (it is related to Cauchy stress by the Piola transformation
 222 $\boldsymbol{\sigma}(\chi(X, t), t) = [J(X, t)]^{-1} \mathbf{P}(X, t) \mathbf{F}^T(X, t)^1$); $\mathbf{b}_R(X, t) = J(X, t) \mathbf{b}(\chi(X, t), t)$ is the body
 223 force per unit volume of \mathcal{B} (whereas \mathbf{b} is the body force per unit volume of \mathcal{C}_t), and collects
 224 both inertial force and long-range interactions; \mathbf{f}_R expresses the contact forces \mathbf{f} , which
 225 act on the boundary of the current configuration, per unit area of $\partial\mathcal{B}$; finally, $\partial\mathcal{B}_N$ is the
 226 Neumann-boundary of \mathcal{B} , i.e. the portion of $\partial\mathcal{B}$ over which surface forces are applied (it
 227 holds that $\partial\mathcal{B}_D \cup \partial\mathcal{B}_N = \partial\mathcal{B}$, and $\partial\mathcal{B}_D \cap \partial\mathcal{B}_N = \emptyset$). The forces \mathbf{f}_R and \mathbf{f} are reciprocally
 228 related by [47]

$$\mathbf{f}_R(X, t) = J(X, t) \mathbf{f}(\chi(X, t), t) \sqrt{\mathbf{N}(X) \cdot \mathbf{C}^{-1}(X, t) \cdot \mathbf{N}(X)}, \quad (X, t) \in \partial\mathcal{B}_N \times \mathcal{J}. \quad (8)$$

229 The left- and the right-hand-side of (7), denoted by $\mathcal{P}_{\text{int}}(\tilde{\mathbf{u}})$ and $\mathcal{P}_{\text{ext}}(\tilde{\mathbf{u}})$, are defined over
 230 $\tilde{\mathcal{H}}$, and are referred to as virtual internal power and virtual external power, respectively.

231 A standard localisation argument associates (7) with its corresponding strong form

$$\text{Div}(\mathbf{P}) = -\mathbf{b}_R, \quad \text{in } \mathcal{B} \times \mathcal{J}, \quad (9a)$$

$$\mathbf{P} \cdot \mathbf{N} = \mathbf{f}_R, \quad \text{on } \partial\mathcal{B}_N \times \mathcal{J}, \quad (9b)$$

$$\mathbf{P} \mathbf{F}^T = \mathbf{F} \mathbf{P}^T, \quad \text{in } \mathcal{B} \times \mathcal{J}. \quad (9c)$$

232 In (9b), \mathbf{N} is the unit vector normal to $\partial\mathcal{B}_N$. Equation (9c) follows from the physical
 233 condition that $\mathcal{P}_{\text{int}}(\tilde{\mathbf{u}})$ must satisfy the Principle of Material Frame Indifference.

234 The dissipation associated with a fixed region $\Omega \in \mathcal{B}$ is defined by [16]

$$\int_{\Omega} D_R = - \overline{\int_{\Omega} \psi_R} + \mathcal{P}_{\text{net}}(\Omega) \geq 0, \quad (10)$$

235 where D_R is the dissipation density, ψ_R is the body's stored energy function, and the net
 236 power $\mathcal{P}_{\text{net}}(\Omega)$ is defined as

$$\mathcal{P}_{\text{net}}(\Omega) = \int_{\partial\Omega} (\mathbf{P} \cdot \mathbf{N}) \cdot \mathbf{u} + \int_{\Omega} \mathbf{b}_R \cdot \mathbf{u} = \int_{\Omega} \mathbf{P} : \mathbf{g} \text{Grad } \mathbf{u}. \quad (11)$$

¹Rigorously speaking, \mathbf{F}^T should be expressed as a functions of x and t . That is, in introducing the Piola transformation of $\boldsymbol{\sigma}$, we are committing the slight abuse of notation $\mathbf{F}^T(X, t) \equiv \mathbf{F}^T(\chi(X, t), t)$.

237 By substituting (11) into (10), and localising the results, one obtains

$$D_{\mathbf{R}} = -\dot{\psi}_{\mathbf{R}} + \mathbf{S} : \frac{1}{2} \dot{\mathbf{C}} \geq 0, \quad (12)$$

238 where $\mathbf{S} = \mathbf{F}^{-1} \mathbf{P} : T^* \mathcal{B} \rightarrow T \mathcal{B}$ is the second Piola-Kirchhoff stress tensor. By introducing
239 the quantities $\psi_{\kappa} = J_{\mathbf{p}}^{-1} \psi_{\mathbf{R}}$ and $D_{\kappa} = J_{\mathbf{p}}^{-1} D_{\mathbf{R}}$, (12) transforms as follows

$$D_{\kappa} = -\dot{\psi}_{\kappa} + \mathbf{S}_{\kappa} : \mathbf{F}_{\mathbf{p}}^{-\mathbf{T}} \frac{1}{2} \dot{\mathbf{C}} \mathbf{F}_{\mathbf{p}}^{-1} \geq 0, \quad (13)$$

240 with $\mathbf{S}_{\kappa} = J_{\mathbf{p}}^{-1} \mathbf{F}_{\mathbf{p}} \mathbf{S} \mathbf{F}_{\mathbf{p}}^{\mathbf{T}}$ being the second Piola-Kirchhoff stress tensor associated with \mathcal{C}_{κ} .

241 3 Constitutive Theory

242 If the material under study is uniform, the constitutive description of its inelastic behaviour
243 can be done by having recourse to the Principle of Material Uniformity [13, 20, 26, 30, 48,
244 49, 50], and the stored energy ψ_{κ} can be expressed constitutively as a function depending
245 solely on the tensor of elastic distortions, $\mathbf{F}_{\mathbf{e}}$, and the hardening variable. Moreover, since
246 constitutive laws must be objective, it must hold that $\hat{\psi}_{\mathbf{R}}(\mathbf{F}, \mathbf{F}_{\mathbf{p}}, \alpha, X) = J_{\mathbf{p}} \hat{\psi}_{\kappa}(\mathbf{C}_{\mathbf{e}}, \alpha)$,
247 with $\mathbf{C}_{\mathbf{e}} = \mathbf{F}_{\mathbf{e}}^{\mathbf{T}} \mathbf{g} \mathbf{F}_{\mathbf{e}}$ being the Cauchy-Green tensor of elastic distortions. The hardening
248 parameter α is introduced with respect to \mathcal{C}_{κ} , and is assumed to be a scalar in the following.

249 3.1 Decoupling of the Stored Energy Function

250 To simplify the forthcoming calculations, the stored energy function $\hat{\psi}_{\kappa}(\mathbf{C}_{\mathbf{e}}, \alpha)$ is given in
251 the decoupled form [15]

$$\hat{\psi}_{\kappa}(\mathbf{C}_{\mathbf{e}}, \alpha) = \hat{W}_{\kappa}(\mathbf{C}_{\mathbf{e}}) + \hat{\mathfrak{H}}_{\kappa}(\alpha), \quad (14)$$

252 where $\hat{\mathfrak{H}}_{\kappa}(\alpha)$ is referred to as hardening potential. By substituting the time derivative of
253 $\hat{\psi}_{\kappa}$ into (13), and hypothesising that the material exhibits hyperelastic behaviour from \mathcal{C}_{κ} ,
254 the following results are obtained:

$$\mathbf{S}_{\kappa} = 2 \frac{\partial \hat{\psi}_{\kappa}}{\partial \mathbf{C}_{\mathbf{e}}} = 2 \frac{\partial \hat{W}_{\kappa}}{\partial \mathbf{C}_{\mathbf{e}}}, \quad (15a)$$

$$\boldsymbol{\Sigma} = \boldsymbol{\eta}^{-1} \mathbf{C}_{\mathbf{e}} \mathbf{S}_{\kappa}, \quad (15b)$$

$$q = -\frac{\partial \hat{\psi}_{\kappa}}{\partial \alpha} = -\frac{\partial \hat{\mathfrak{H}}_{\kappa}}{\partial \alpha}, \quad (15c)$$

$$D_{\kappa} = \boldsymbol{\Sigma} : \boldsymbol{\eta} \mathbf{L}_{\mathbf{p}} + q \dot{\alpha} \geq 0. \quad (15d)$$

255 Given \hat{W}_{κ} and $\hat{\mathfrak{H}}_{\kappa}$ explicitly, \mathbf{S}_{κ} , the Mandel stress tensor $\boldsymbol{\Sigma}$, and the generalised force
256 q dual to the hardening rate $\dot{\alpha}$ are expressed constitutively by (15a), (15b) and (15c),
257 respectively. Since it has been assumed that anelastic (plastic) distortions are isochoric,
258 $\mathbf{L}_{\mathbf{p}}$ is trace-free, which implies that only the deviatoric part of $\boldsymbol{\Sigma}$ is constrained by the
259 residual dissipation inequality (15d). Moreover, a consequence of the decoupled form of
260 the stored energy function is that the stress does not depend on the hardening function
261 and, similarly, the force-like variable q does not depend on deformation.

262 3.2 Isotropy

263 Although there exist theoretical models and computational algorithms elaborated for
264 finite-strain elastoplasticity of anisotropic materials (cf., e.g., [51, 52, 53, 54, 55]), the

majority of the numerical methods rely, to the authors' knowledge, on the hypothesis of isotropic material behaviour [2, 15, 24, 46, 56].

There are at least two big advantages implied by isotropy. The first one is that the issue of plastic spin does not arise at all (see, e.g., [30]); the second advantage is that the flow rule can be formulated in terms of \mathbf{B}_p , so that no evolution law for \mathbf{F}_p is actually needed (in some cases —e.g., for polycrystals [57]— evolution laws for \mathbf{F}_p are prescribed, in accordance to Mandel's isoclinicity rule [2], under the assumption of vanishing plastic rotations, so that the plastic variable is either \mathbf{V}_p or \mathbf{U}_p , depending on whether the right or the left decomposition of $\mathbf{F}_p = \mathbf{R}_p \mathbf{U}_p = \mathbf{V}_p \mathbf{R}_p$ is chosen).

For a hyperelastic isotropic material, the stored energy function \hat{W}_κ depends on \mathbf{C}_e exclusively through its invariants, i.e.

$$I_1 = \hat{I}_1(\mathbf{C}_e) = \text{tr}(\boldsymbol{\eta}^{-1} \mathbf{C}_e) = \text{tr}(\mathbf{B}_p \mathbf{C}), \quad (16a)$$

$$I_2 = \hat{I}_2(\mathbf{C}_e) = \frac{1}{2} \{ [\hat{I}_1(\mathbf{C}_e)]^2 - \text{tr}[(\boldsymbol{\eta}^{-1} \mathbf{C}_e)^2] \} = \frac{1}{2} \{ I_1^2 - \text{tr}(\mathbf{B}_p \mathbf{C} \mathbf{B}_p \mathbf{C}) \}, \quad (16b)$$

$$I_3 = \hat{I}_3(\mathbf{C}_e) = \det(\mathbf{C}_e) = J^2. \quad (16c)$$

This property necessarily implies that the Mandel stress tensor $\boldsymbol{\Sigma}$, which by definition must satisfy the equality $\boldsymbol{\Sigma} \mathbf{C}_e \boldsymbol{\eta}^{-1} = \boldsymbol{\eta}^{-1} \mathbf{C}_e \boldsymbol{\Sigma}^T$ (cf. (15b)), must be symmetric itself, i.e. $\boldsymbol{\Sigma} = \boldsymbol{\Sigma}^T$. Indeed, by setting $\hat{W}_\kappa(\mathbf{C}_e) = \hat{W}_\kappa(\hat{I}_1(\mathbf{C}_e), \hat{I}_2(\mathbf{C}_e), \hat{I}_3(\mathbf{C}_e))$, one obtains

$$\boldsymbol{\Sigma} = 2\beta_1 \boldsymbol{\eta}^{-1} \mathbf{C}_e \boldsymbol{\eta}^{-1} + 2\beta_2 [I_1 \boldsymbol{\eta}^{-1} \mathbf{C}_e \boldsymbol{\eta}^{-1} - \boldsymbol{\eta}^{-1} \mathbf{C}_e \boldsymbol{\eta}^{-1} \mathbf{C}_e \boldsymbol{\eta}^{-1}] + 2\beta_3 I_3 \boldsymbol{\eta}^{-1}, \quad (17)$$

with $\{\beta_i = \frac{\partial \hat{W}_\kappa}{\partial I_i}\}_{i=1}^3$. Since $\boldsymbol{\Sigma}$ is symmetric, the first summand on the right-hand-side of (15d) becomes $\boldsymbol{\Sigma} : \boldsymbol{\eta} \mathbf{L}_p = \boldsymbol{\Sigma} : \mathbf{D}_p$, meaning that only the symmetric part of the rate of plastic distortions contributes to dissipation. This result rules out the plastic spin, i.e. the skew-symmetric part of $\boldsymbol{\eta} \mathbf{L}_p$, which cannot thus be determined in terms of thermodynamic arguments [30]. Finally, by invoking the kinematic relations (3), the inequality (15d) can be rewritten as

$$D_\kappa = -\frac{1}{2} (\mathbf{g} \text{dev}(\boldsymbol{\tau}_\kappa) \mathbf{b}_e^{-1}) : \mathcal{L}_v \mathbf{b}_e + q \dot{\alpha} \geq 0, \quad (18)$$

where $\boldsymbol{\tau}_\kappa = \mathbf{F}_e \mathbf{S}_\kappa \mathbf{F}_e^T = \mathbf{g}^{-1} \mathbf{F}_e^{-T} \boldsymbol{\eta} \boldsymbol{\Sigma} \mathbf{F}_e^T$ is the Kirchhoff stress tensor associated with the body's natural state. Furthermore, setting $\boldsymbol{\tau} = J_p \boldsymbol{\tau}_\kappa$ (with $J_p = 1$), it is also useful to introduce the material Mandel stress tensor $\boldsymbol{\Sigma}_R = \mathbf{G}^{-1} \mathbf{F}^T \mathbf{g} \boldsymbol{\tau} \mathbf{F}^{-T}$. The constitutive expressions of $\boldsymbol{\tau}_\kappa$ and $\boldsymbol{\Sigma}_R$ read

$$\hat{\boldsymbol{\tau}}_\kappa(\mathbf{F}, \mathbf{B}_p) = 2\beta_1 \mathbf{b}_e + 2\beta_2 (I_1 \mathbf{b}_e - \mathbf{b}_e \mathbf{g} \mathbf{b}_e) + 2\beta_3 I_3 \mathbf{g}^{-1}, \quad (19a)$$

$$\hat{\boldsymbol{\Sigma}}_R(\mathbf{F}, \mathbf{B}_p) = (2\beta_1 + 2\beta_2 I_1) \mathbf{G}^{-1} \mathbf{C} \mathbf{B}_p - 2\beta_2 \mathbf{G}^{-1} \mathbf{C} \mathbf{B}_p \mathbf{C} \mathbf{B}_p + 2\beta_3 I_3 \mathbf{G}^{-1}. \quad (19b)$$

The tensor $\boldsymbol{\Sigma}_R$ is not symmetric in general, but it has the properties $\boldsymbol{\Sigma}_R \mathbf{C} \mathbf{G}^{-1} = (\boldsymbol{\Sigma}_R \mathbf{C} \mathbf{G}^{-1})^T$, $\mathbf{G} \boldsymbol{\Sigma}_R \mathbf{B}_p^{-1} = (\mathbf{G} \boldsymbol{\Sigma}_R \mathbf{B}_p^{-1})^T$ and $\mathbf{B}_p \mathbf{G} \boldsymbol{\Sigma}_R = (\mathbf{B}_p \mathbf{G} \boldsymbol{\Sigma}_R)^T$. The first one follows from its own definition, while the second and the third one follow from isotropy [30].

3.3 Rate-Independent Plasticity and Yield Criterion

The hypothesis of rate-independent plasticity requires the introduction of a yield criterion [16]. To this end, let \mathcal{T}_τ and \mathcal{T}_q be the spaces of Kirchhoff stresses and stress-like hardening functions q (cf. (15c)), and let $f_\tau : \mathcal{T}_\tau \times \mathcal{T}_q \rightarrow \mathbb{R}$ be a yield function defined by

$$f_\tau(\boldsymbol{\tau}_\kappa, q) = \varphi_\tau(\text{dev}(\boldsymbol{\tau}_\kappa)) + \sqrt{\frac{2}{3}} [q - \tau_y], \quad (20)$$

where the positive parameter τ_y is the yield stress, and the function φ_τ depends on $\boldsymbol{\tau}_\kappa$ through the deviatoric part of it for consistency with (18).

298 The set $\mathcal{A} = \{(\boldsymbol{\tau}_\kappa, q) \in \mathcal{T}_\tau \times \mathcal{J}_q : f_\tau(\boldsymbol{\tau}_\kappa, q) \leq 0\}$ is referred to as the set of admissible
 299 stresses. In accordance with von Mises classical theory of J_2 -plasticity, the function φ_τ
 300 defined here as $\varphi_\tau(\text{dev}(\boldsymbol{\tau}_\kappa)) = \|\text{dev}(\boldsymbol{\tau}_\kappa)\| = \sqrt{\text{tr}[(\mathbf{g}\text{dev}(\boldsymbol{\tau}_\kappa))^2]}$. Consequently, one obtains

$$\frac{\partial f_\tau}{\partial \boldsymbol{\tau}_\kappa}(\boldsymbol{\tau}_\kappa, q) = \mathbf{g}\mathbf{n}\mathbf{g} \equiv \mathbf{n}^b, \quad \mathbf{n} = \frac{\text{dev}(\boldsymbol{\tau}_\kappa)}{\|\text{dev}(\boldsymbol{\tau}_\kappa)\|}, \quad (21)$$

301 with $\|\mathbf{n}\| = 1$. The inequality $f_\tau(\boldsymbol{\tau}_\kappa, q) < 0$ defines the instantaneous elastic range of the
 302 material. Plastic flow begins when the boundary of \mathcal{A} is reached, i.e. when $f_\tau(\boldsymbol{\tau}_\kappa, q) = 0$.

303 3.4 Principle of Maximum Plastic Dissipation and Flow Rules

304 To formulate the Principle of Maximum Plastic Dissipation (PMPD), the dissipation \mathcal{D}_κ
 305 (cf. (18)) has to be viewed as a non-negative, real-valued function defined over the set
 306 \mathcal{A} . The PMPD affirms that D_κ reaches its maximum when it is computed for the actual
 307 values of stress $\boldsymbol{\tau}_\kappa$ and hardening function q that characterise the material, i.e.

$$D_\kappa(\boldsymbol{\tau}_\kappa, q) = \max_{(\mathbf{r}, \vartheta) \in \mathcal{A}} \{D_\kappa(\mathbf{r}, \vartheta)\}. \quad (22)$$

308 Since the maximisation is performed under the constraint that the pair $(\mathbf{r}, \vartheta) \in \mathcal{A}$ be
 309 admissible, the condition (22) allows to reformulate (18) into a constrained optimisation
 310 problem, which can be studied by introducing the Lagrangian function

$$L_\kappa(\mathbf{r}, \vartheta, \gamma_\tau) = D_\kappa(\mathbf{r}, \vartheta) - \gamma_\tau f_\tau(\mathbf{r}, \vartheta), \quad (\mathbf{r}, \vartheta) \in \mathcal{A}, \quad (23)$$

311 where γ_τ is an unknown Lagrange multiplier. Maximising (23) leads to the optimality
 312 conditions [15, 46]

$$\mathcal{L}_v \mathbf{b}_e = -2\gamma_\tau \mathbf{n}\mathbf{g}\mathbf{b}_e, \quad (24a)$$

$$\dot{\alpha} = \gamma_\tau \sqrt{\frac{2}{3}}, \quad (24b)$$

$$\gamma_\tau \geq 0, \quad f_\tau(\boldsymbol{\tau}_\kappa, q) \leq 0, \quad \gamma_\tau f_\tau(\boldsymbol{\tau}_\kappa, q) = 0. \quad (24c)$$

313 Equations (24) determine the Karush-Kuhn-Tucker (KKT) system, and are also referred
 314 to as KKT-conditions. By invoking (3a), (24a) can be rewritten in terms of $\dot{\mathbf{B}}_p$, i.e.

$$\dot{\mathbf{B}}_p = -2\gamma_\tau \mathbf{F}^{-1}(\mathbf{n}\mathbf{g}\mathbf{b}_e)\mathbf{F}^{-T}. \quad (25)$$

315 A consequence of (19a) is that the product $\mathbf{n}\mathbf{g}\mathbf{b}_e$ is commutative. Moreover, by recalling
 316 the identity $\text{dev}(\boldsymbol{\tau}) = \mathbf{g}^{-1}\mathbf{F}^{-T}\mathbf{G}\text{dev}(\boldsymbol{\Sigma}_R)\mathbf{F}^T$, (25) becomes

$$\dot{\mathbf{B}}_p = -2\gamma_\tau \mathbf{B}_p \mathbf{G} \frac{\text{dev}(\boldsymbol{\Sigma}_R)}{\|\text{dev}(\boldsymbol{\tau})\|}. \quad (26)$$

317 According to (24c), γ_τ is zero when the material is in its elastic range, i.e. when
 318 $f_\tau(\boldsymbol{\tau}_\kappa, q) < 0$, and is greater than zero, when the yield surface is reached, i.e. when
 319 $f_\tau(\boldsymbol{\tau}_\kappa, q) = 0$. In the case in which γ_τ is positive, it is determined by the consistency
 320 condition $\gamma_\tau \dot{f}_\tau(\boldsymbol{\tau}_\kappa, q) = 0$, which leads to the expression

$$\gamma_\tau = \frac{\mathbf{n}^b : J_{e^A} : \mathbf{d}}{\mathbf{n}^b : J_{e^A} : \mathbf{n}^b + (2/3)\partial_\alpha^2 \hat{\mathcal{J}}_\kappa} = \frac{-\mathbf{n}^b : J_{e^{\mathbb{B}_p}} : \frac{1}{2}\mathcal{L}_v \mathbf{b}_e}{\mathbf{n}^b : J_{e^A} : \mathbf{n}^b}, \quad (27)$$

321 with

$$J_e \mathbb{A} = J_e \mathbb{C} + \boldsymbol{\tau}_\kappa \otimes \bar{\mathbf{g}}^{-1} + \mathbf{g}^{-1} \otimes \boldsymbol{\tau}_\kappa, \quad (28a)$$

$$J_e \mathbb{C} = \mathbf{F}_e \otimes \mathbf{F}_e : \mathbb{C}_\kappa : \mathbf{F}_e^T \otimes \mathbf{F}_e^T, \quad \mathbb{C}_\kappa = 4 \frac{\partial^2 \hat{W}_\kappa}{\partial \mathbf{C}_e^2}(\mathbf{C}_e), \quad (28b)$$

$$J_{\mathbb{B}_p} = \mathbf{F} \otimes \mathbf{F} : \mathbb{B}_p : \mathbf{F}^{-1} \otimes \mathbf{F}^{-1}, \quad \mathbb{B}_p = 2 \frac{\partial \hat{\mathcal{S}}}{\partial \mathbf{B}_p}(\mathbf{C}, \mathbf{B}_p). \quad (28c)$$

322 The fourth-order tensors \mathbb{A} and \mathbb{C} are referred to as tensor of the effective elastic moduli
 323 and spatial elasticity tensor, respectively. Moreover, $\mathbf{S} = \hat{\mathbf{S}}(\mathbf{C}, \mathbf{B}_p) = J_p \mathbf{F}_p^{-1} \mathbf{S}_\kappa \mathbf{F}_p^{-T}$ is
 324 the constitutive expression of the material second Piola-Kirchhoff stress tensor. According
 325 to (27), the multiplier γ_τ (when it is nonzero) is defined as a function of \mathbf{F} , $\dot{\mathbf{F}}$, \mathbf{B}_p and α ,
 326 i.e. $\gamma_\tau = \hat{\gamma}_\tau(\mathbf{F}, \dot{\mathbf{F}}, \mathbf{B}_p, \alpha)$.

327 In conclusion, equations (24a) and (24b), largely adopted in von Mises J_2 -theory of
 328 Elastoplasticity, can be reformulated as evolution laws for the plastic variables \mathbf{B}_p and α :

$$\dot{\mathbf{B}}_p = \begin{cases} -\hat{\mathcal{R}}(\mathbf{F}, \dot{\mathbf{F}}, \mathbf{B}_p, \alpha), & \text{if } \gamma_\tau = \hat{\gamma}_\tau(\mathbf{F}, \dot{\mathbf{F}}, \mathbf{B}_p, \alpha) > 0 \quad (f_\tau(\boldsymbol{\tau}_\kappa, q) = 0), \\ \mathbf{0} & \text{if } \gamma_\tau = 0, \quad (f_\tau(\boldsymbol{\tau}_\kappa, q) < 0), \end{cases} \quad (29a)$$

$$\dot{\alpha} = \begin{cases} \sqrt{\frac{2}{3}} \hat{\gamma}_\tau(\mathbf{F}, \dot{\mathbf{F}}, \mathbf{B}_p, \alpha), & \text{if } \gamma_\tau = \hat{\gamma}_\tau(\mathbf{F}, \dot{\mathbf{F}}, \mathbf{B}_p, \alpha) > 0 \quad (f_\tau(\boldsymbol{\tau}_\kappa, q) = 0), \\ 0 & \text{if } \gamma_\tau = 0, \quad (f_\tau(\boldsymbol{\tau}_\kappa, q) < 0), \end{cases} \quad (29b)$$

329 where the negative of the tensor-valued function $\hat{\mathcal{R}}$ is defined by the right-hand-side of (26).
 330 Clearly, the definition of $\hat{\mathcal{R}}$ depends on the choice of the stored energy density function
 331 \hat{W}_κ , and of the hardening potential $\hat{\mathcal{H}}_\kappa$.

332 3.5 Other Types of Flow Rules

333 In some biomechanical contexts, as those addressing the structural reorganisation of cell
 334 aggregates, plasticity-like models have been developed in which hardening is usually not
 335 accounted for, and the anelastic distortions model the reorganisation of the adhesion bonds
 336 connecting the cells. The onset of this type of anelastic processes is taken into account
 337 by introducing a yield stress in the constitutive laws. The symmetric part of the rate of
 338 plastic distortions is driven by stress according to laws of the type [58]

$$\mathbf{D}_p = \zeta_p \boldsymbol{\eta} \operatorname{dev}(\boldsymbol{\Sigma}) \boldsymbol{\eta} = \zeta_p \mathbf{F}_e^T \mathbf{g} \operatorname{dev}(\boldsymbol{\tau}_\kappa) \mathbf{F}_e^{-T} \boldsymbol{\eta}, \quad (30)$$

339 where ζ_p is a plastic multiplier. By invoking (3b), the flow rule (30) becomes

$$\dot{\mathbf{B}}_p = -2 (J_p^{-1} \zeta_p) \mathbf{B}_p \mathbf{G} \operatorname{dev}(\boldsymbol{\Sigma}_R). \quad (31)$$

340 In (30) and (31), ζ_p is defined by²

$$\zeta_p = J_p \lambda \left[\frac{\varphi(\boldsymbol{\tau}) - \sqrt{(2/3)} \tau_y}{\varphi(\boldsymbol{\tau})} \right]_+, \quad (32)$$

341 where λ is a non-negative phenomenological coefficient (with units $[\lambda] = (\text{s} \cdot \text{MPa})^{-1}$),
 342 $[\mathbf{f}]_+ = \mathbf{f}$, if $\mathbf{f} > 0$, and $[\mathbf{f}]_+ = 0$ otherwise, and $\varphi(\boldsymbol{\tau}) = \|\operatorname{dev}(\boldsymbol{\tau})\|$. Since the constraint

²The definition of γ_p given in [58] is slightly different from that reported here, where the expression of γ_p in (32) has been introduced for consistency with the rest of the paper.

343 $J_p = 1$ applies, it holds that $\boldsymbol{\tau} = \boldsymbol{\tau}_\kappa$, and (31) becomes

$$\dot{\mathbf{B}}_p = -2\gamma_p \mathbf{B}_p \mathbf{G} \frac{\text{dev}(\boldsymbol{\Sigma}_R)}{\|\text{dev}(\boldsymbol{\tau})\|}, \quad (33a)$$

$$\gamma_p := \lambda \left[\|\text{dev}(\boldsymbol{\tau})\| - \sqrt{(2/3)\tau_y} \right]_+, \quad (33b)$$

344 with $[\gamma_p] = s^{-1}$. Although γ_p is not a Lagrange multiplier, since it does not have to comply
 345 with a consistency condition of the type (27), the flow rule (33a) satisfies the dissipation
 346 inequality. Moreover, comparing (33a) with (26), one can show that the two flow rules are
 347 identical up to the specification of γ_τ and γ_p . Thus, the right-hand-side of (33a) can be
 348 expressed by means of a tensor-valued function $\hat{\mathbf{R}}(\mathbf{F}, \mathbf{B}_p)$. The dependence on $\dot{\mathbf{F}}$ does not
 349 appear, since γ_p is not restricted by any KKT-consistency condition of the type (27).

350 4 Statement and Solution of the Problems ‘Pr1’ and ‘Pr2’

351 For simplicity, the external forces \mathbf{b}_R and \mathbf{f}_R are set equal to zero from here on. Thus,
 352 it holds $\mathbf{P} \cdot \mathbf{N} = \mathbf{0}$ on $\partial\mathcal{B}_N$ (cf. (9b)). Consequently, the problem ‘Pr1’ can be stated as
 353 follows:

354 4.1 Problem ‘Pr1’

355 Let $\hat{W}_\kappa(\mathbf{C}_e)$, $\hat{\mathcal{H}}_\kappa(\alpha)$, f_τ , γ_τ , and \mathcal{R} be given such that

$$\mathbf{P} = \hat{\mathbf{P}}(\mathbf{F}, \mathbf{B}_p) = J_p \hat{\boldsymbol{\tau}}_\kappa(\mathbf{F}, \mathbf{B}_p) \mathbf{F}^{-\text{T}} = J_p \left[\mathbf{F}_e \left(2 \frac{\partial \hat{W}_\kappa}{\partial \mathbf{C}_e}(\mathbf{C}_e) \right) \mathbf{F}_e^\text{T} \right] \mathbf{F}^{-\text{T}}, \quad (34a)$$

$$q = -K(\alpha) = -\frac{\partial \hat{\mathcal{H}}_\kappa}{\partial \alpha}(\alpha), \quad (34b)$$

$$\gamma_\tau = \begin{cases} 0, & \text{if } f_\tau(\boldsymbol{\tau}_\kappa, q) < 0, \\ \hat{\gamma}_\tau(\mathbf{F}, \dot{\mathbf{F}}, \mathbf{B}_p, \alpha) > 0, & \text{if } f_\tau(\boldsymbol{\tau}_\kappa, q) = 0, \end{cases} \quad (34c)$$

$$\mathcal{R} = \begin{cases} \mathbf{0}, & \text{if } f_\tau(\boldsymbol{\tau}_\kappa, q) < 0, \\ \hat{\mathbf{R}}(\mathbf{F}, \dot{\mathbf{F}}, \mathbf{B}_p, \alpha), & \text{if } f_\tau(\boldsymbol{\tau}_\kappa, q) = 0, \end{cases} \quad (34d)$$

356 where $\hat{\gamma}_\tau$ and $\hat{\mathbf{R}}$ are known functions of their arguments, with $\hat{\mathbf{R}}$ being specified in (25).

357

Find $\chi \in \mathcal{H}$, $\mathbf{B}_p \in \mathbf{L}^2(\mathcal{B} \times \mathcal{J}, T\mathcal{B} \otimes T\mathcal{B})$ and $\alpha \in L^2(\mathcal{B} \times \mathcal{J}, \mathbb{R})$ such that

$$\mathcal{P}(\chi, \mathbf{B}_p, \tilde{\mathbf{u}}) := \int_{\mathcal{B}} \hat{\mathbf{P}}(\mathbf{F}, \mathbf{B}_p) : \mathbf{g} \text{Grad } \tilde{\mathbf{u}} = 0, \quad \forall \tilde{\mathbf{u}} \in \tilde{\mathcal{H}}, \quad (35a)$$

$$\dot{\mathbf{B}}_p = -\mathcal{R}, \quad \mathbf{B}_p(X, 0) = \mathbf{B}_{p0}(X) \text{ in } \mathcal{B}, \quad (35b)$$

$$\dot{\alpha} = \gamma_\tau \sqrt{\frac{2}{3}}, \quad \alpha(X, 0) = \alpha_0(X) \text{ in } \mathcal{B}. \quad (35c)$$

359

360 Here, $\mathbf{L}^2(\mathcal{B} \times \mathcal{J}, T\mathcal{B} \otimes T\mathcal{B})$ and $L^2(\mathcal{B} \times \mathcal{J}, \mathbb{R})$ denote, respectively, the spaces of all tensor-
 361 valued and scalar-valued functions that are (Lebesgue) square-integrable in \mathcal{B} , while \mathcal{H} is
 362 the subset of $(H^1(\mathcal{B} \times \mathcal{J}, \mathcal{S}))^3$ characterised by the property

$$\mathcal{H} = \left\{ \chi \in (H^1(\mathcal{B} \times \mathcal{J}, \mathcal{S}))^3 : \chi(X, t) = \chi_b(t), \forall (X, t) \in \partial\mathcal{B}_D \times \mathcal{J} \right\}, \quad (36)$$

363 with $(H^1(\mathcal{B} \times \mathcal{J}, \mathcal{S}))^3$ being the Sobolev space of all functions $\chi(\cdot, t)$, $t \in \mathcal{J}$, valued in
 364 the three-dimensional Euclidean space \mathcal{S} that are square-integrable in \mathcal{B} and whose weak

365 derivatives $D^k \chi(\cdot, t)$, with $|k| \leq 1$, are all square-integrable in \mathcal{B} , too (here, k denotes
366 a multi-index) [59]. Moreover, in (36), χ_b is the prescribed value of the motion on the
367 body's Dirichlet-boundary $\partial\mathcal{B}_D$. The space of virtual velocities $\tilde{\mathcal{H}}$ can now be identified
368 with the functional space $(H_0^1(\mathcal{B}, \mathcal{S}))^3$, i.e. $\tilde{\mathcal{H}} = (H_0^1(\mathcal{B}, \mathcal{S}))^3$, which is the Hilbert sub-
369 space of $(H^1(\mathcal{B}, \mathcal{S}))^3$ defined as the closure of the space of test-functions in $(H^1(\mathcal{B}, \mathcal{S}))^3$,
370 and characterised by the property that all functions $\tilde{\mathbf{u}} \in (H_0^1(\mathcal{B}, \mathcal{S}))^3$ vanish on $\partial\mathcal{B}_D$ [59].

371 The problem ‘Pr1’ (formulated by (34a)–(35c)) stems from the von Mises J_2 theory of
372 isochoric and associative plasticity, since the rate of plastic distortions is deviatoric and
373 proportional to the associated measure of stress. On the other hand, granted isotropy,
374 and provided that \mathcal{R} complies with some restrictions related to dissipation (e.g., resid-
375 ual dissipation inequality [15], or maximisation of plastic work [2]), equation (35b) can
376 also be generalised to comprehend many other types of flow rules, which might be even
377 fully phenomenological, and need not be associative in general. For this reason, it is also
378 useful to consider modified versions of ‘Pr1’, which do not strictly follow from the KKT-
379 conditions (24), like, for instance, the problem referred to as ‘Pr2’ in this paper.

380 4.2 Problem ‘Pr2’

381 Let $\hat{W}_\kappa(\mathbf{C}_e)$ and $\hat{\mathcal{R}}(\mathbf{F}, \mathbf{B}_p)$ be given, and let the first Piola-Kirchhoff stress tensor be defined
382 by

$$\mathbf{P} = \hat{\mathbf{P}}(\mathbf{F}, \mathbf{B}_p) = J_p \hat{\boldsymbol{\tau}}_\kappa(\mathbf{F}, \mathbf{B}_p) \mathbf{F}^{-T} = J_p \left[\mathbf{F}_e \left(2 \frac{\partial \hat{W}_\kappa}{\partial \mathbf{C}_e}(\mathbf{C}_e) \right) \mathbf{F}_e^T \right] \mathbf{F}^{-T}. \quad (37)$$

383

Find $\chi \in \mathcal{H}$ and $\mathbf{B}_p \in \mathbf{L}^2(\mathcal{B} \times \mathcal{J}, T\mathcal{B} \otimes T\mathcal{B})$ such that

$$\mathcal{P}(\chi, \mathbf{B}_p, \tilde{\mathbf{u}}) := \int_{\mathcal{B}} \hat{\mathbf{P}}(\mathbf{F}, \mathbf{B}_p) : \mathbf{g} \text{Grad } \tilde{\mathbf{u}} = 0, \quad \forall \tilde{\mathbf{u}} \in \tilde{\mathcal{H}}, \quad (38a)$$

384

$$\dot{\mathbf{B}}_p = -\hat{\mathcal{R}}(\mathbf{F}, \mathbf{B}_p), \quad \mathbf{B}_p(X, 0) = \mathbf{B}_{p0}(X) \text{ in } \mathcal{B}. \quad (38b)$$

385

386 The tensor-valued function $\hat{\mathcal{R}}$ of the flow rule (38b) can be given, for example, by the
387 right-hand-side of (33a), with γ_p defined in (33b) [58], or by more general expressions that
388 lead to non-associative plasticity [2].

389 5 A Review of the Return Mapping Algorithm for ‘Pr1’

390 Looking at some literature (see, e.g., [15, 46, 60]), the RMA is usually formulated under
391 two hypotheses, which add themselves to those discussed in sections 3.1–3.4. The first
392 hypothesis is that the strain energy density $\hat{W}_\kappa(\mathbf{C}_e)$ used in ‘Pr1’, can be decoupled into
393 a pure volumetric contribution, $\hat{U}_\kappa(J_e)$, and a purely isochoric contribution, $\overline{W}_\kappa(\overline{\mathbf{C}}_e)$. In
394 particular, a quasi-incompressible Neo-Hookean material is considered, i.e.

$$\hat{W}_\kappa(\mathbf{C}_e) = \hat{U}_\kappa(J_e) + \overline{W}_\kappa(\overline{\mathbf{C}}_e), \quad (39a)$$

$$\hat{U}_\kappa(J_e) = \frac{1}{2} \kappa \left\{ \frac{1}{2} (J_e^2 - 1) - \ln(J_e) \right\}, \quad (39b)$$

$$\overline{W}_\kappa(\overline{\mathbf{C}}_e) = \frac{1}{2} \mu \left\{ \text{tr}(\boldsymbol{\eta}^{-1} \overline{\mathbf{C}}_e) - 3 \right\}, \quad (39c)$$

395 where κ and μ are the bulk and shear moduli, respectively, and $\mathbf{C}_e = J_e^{2/3} \overline{\mathbf{C}}_e$ [32, 33], with
396 $\det(\overline{\mathbf{C}}_e) = 1$. In (39a)–(39c), as well as in all the following calculations, both $J_e = \sqrt{\det(\mathbf{C}_e)}$
397 and $\overline{\mathbf{C}}_e$ are to be regarded as functions of \mathbf{C}_e . Direct consequences of this hypothesis are the
398 equalities $\beta_1 = \frac{\mu}{2} J_e^{-2/3}$ and $\beta_2 = 0$, which lead to $\text{dev}(\boldsymbol{\tau}_\kappa) = \mu \text{dev}(\overline{\mathbf{b}}_e)$, with $\overline{\mathbf{b}}_e = J_e^{-2/3} \mathbf{b}_e$.

399 The second hypothesis is that the right-hand-side of (24a) can be approximated by
 400 $\frac{1}{3}\text{tr}(\mathbf{g}\mathbf{b}_e)\mathbf{n}$, so that the flow rule becomes

$$\mathcal{L}_v \mathbf{b}_e = -\frac{2}{3}\gamma_\tau \text{tr}(\mathbf{g}\mathbf{b}_e)\mathbf{n}. \quad (40)$$

401 This is obtained by enforcing the decomposition $\mathbf{b}_e = \frac{1}{3}\text{tr}(\mathbf{g}\mathbf{b}_e)\mathbf{g}^{-1} + \text{dev}(\mathbf{b}_e)$ in (24a), and
 402 neglecting the term $\mathbf{n}\mathbf{g}\text{dev}(\mathbf{b}_e)$ with respect to the right-hand-side of (40). To justify this
 403 approximation it suffices to notice that, when plastic flow occurs (i.e. when the condition
 404 $f_\tau(\boldsymbol{\tau}_\kappa, q) = 0$ is satisfied), $\mathbf{n}\mathbf{g}\text{dev}(\mathbf{b}_e)$ becomes

$$\mathbf{n}\mathbf{g}\text{dev}(\mathbf{b}_e) = J_e^{2/3} \frac{\|\text{dev}(\boldsymbol{\tau}_\kappa)\|}{\mu} \mathbf{n}\mathbf{g}\mathbf{n} = J_e^{2/3} \frac{\sqrt{\frac{2}{3}}(K(\alpha) + \tau_y)}{\mu} \mathbf{n}\mathbf{g}\mathbf{n}. \quad (41)$$

405 This result amounts to say that the term $\mathbf{n}\mathbf{g}\text{dev}(\mathbf{b}_e)$ can be dropped because it is of the
 406 same order as the ratio between the yield stress in the presence of hardening, $\sqrt{\frac{2}{3}}(K(\alpha) +$
 407 $\tau_y)$, and the shear modulus, which is usually small for the majority of metals [46]. Even
 408 though, as stated by Simo [46], this approximation is not essential, it simplifies considerably
 409 the numerical treatment of the flow rule and the determination of γ_τ .

410 Although the strain energy density (39) reduces the computational effort (since it is
 411 independent of I_2), it might be unrealistic in some situations. In fact, it applies to elastically
 412 quasi-incompressible materials (for which J_e is close to unity), but fails to reproduce the
 413 correct elastic response of materials for which this assumption cannot be done. Indeed,
 414 the use of (39) for materials not satisfying quasi-incompressibility suppresses unjustifiably
 415 some independent elastic parameters from the material's elasticity tensor [61, 62, 63, 64,
 416 65].

417 5.1 Algorithmic Determination of the KKT-Multiplier

418 This Section largely follows the theory reported in [15]. The crux of the RMA is describing
 419 the time-discrete evolution of \mathbf{B}_p and α jointly with the discretised KKT-conditions (24)
 420 and the weak form of the momentum balance (35a). For this purpose, at each instant of
 421 time $t_n \in \mathcal{J}$, $n \in \mathbb{N}$, the body is assumed to be characterised by two states: The *actual state*
 422 is that determined by the functions χ_n , \mathbf{B}_{pn} and α_n , which represent the actual solution of
 423 ‘Pr1’ at time t_n . The *trial state*, instead, is the one in which the body would find itself, if
 424 no plastic evolution took place within the time step $\Delta t_n = t_n - t_{n-1}$, $n \geq 1$. By definition,
 425 the trial state is determined by the functions χ_n^{trial} , $\mathbf{B}_{pn}^{\text{trial}} = \mathbf{B}_{p(n-1)}$ and $\alpha_n^{\text{trial}} = \alpha_{n-1}$,
 426 where χ_n^{trial} is the solution to (35a) at time t_n , if \mathbf{B}_{pn} were substituted in the constitutive
 427 expression of the first Piola-Kirchhoff stress tensor with the stepwise constant function
 428 $\mathbf{B}_{p(n-1)}$ [15].

429 The introduction of the trial state, the particularly simple strain energy density specified
 430 in (39), and the approximated flow rule (40) allow to express the time-discrete form of (40)
 431 in terms of stress and, above all, to consider the stress at time t_n as a function of the
 432 deformation gradient and trial quantities only.

433 By recalling (3a), the Lie-derivative of \mathbf{b}_e at time $t_n \in \mathcal{J}$ is approximated by

$$(\mathcal{L}_v \mathbf{b}_e)_n = \mathbf{F}_n \frac{\mathbf{B}_{pn} - \mathbf{B}_{p(n-1)}}{\Delta t_n} \mathbf{F}_n^T, \quad n \in \mathbb{N}, n \geq 1, \quad (42)$$

434 where \mathbf{F}_n is the tangent map of χ_n , and the time derivative $\dot{\mathbf{B}}_p$ has been replaced by a
 435 finite difference. Moreover, substituting (42) into the left-hand-side of (40) leads to [15]

$$\bar{\mathbf{b}}_{en} = \bar{\mathbf{b}}_{en}^{\text{trial}} - \frac{2}{3}\gamma_\tau n \Delta t_n \text{tr}(\mathbf{g}\bar{\mathbf{b}}_{en}) \mathbf{n}_n, \quad (43)$$

436 with $\bar{\mathbf{b}}_{en} = J_{en}^{-2/3} \mathbf{b}_{en}$, $\mathbf{b}_{en} = \mathbf{F}_n \mathbf{B}_{pn} \mathbf{F}_n^T$, $\bar{\mathbf{b}}_{en}^{\text{trial}} = J_{en}^{-2/3} \mathbf{b}_{en}^{\text{trial}}$, and $\mathbf{b}_{en}^{\text{trial}} = \mathbf{F}_n \mathbf{B}_{p(n-1)} \mathbf{F}_n^T$,
 437 which implies that $\text{tr}(\mathbf{g}\bar{\mathbf{b}}_{en}) = \text{tr}(\mathbf{g}\bar{\mathbf{b}}_{en}^{\text{trial}})$. Hence, taking the deviatoric part of both sides
 438 of (43), and multiplying the resulting expression by μ , one obtains

$$\mathbf{s}_n = \mathbf{s}_n^{\text{trial}} - \frac{2}{3} \mu \gamma_{\tau n} \Delta t_n \text{tr}(\mathbf{g}\bar{\mathbf{b}}_{en}^{\text{trial}}) \mathbf{n}_n, \quad (44)$$

439 where the notation $\mathbf{s}_n = \text{dev}(\boldsymbol{\tau}_{\kappa n}) = \mu \text{dev}(\bar{\mathbf{b}}_{en})$, and $\mathbf{s}_n^{\text{trial}} = \mu \text{dev}(\bar{\mathbf{b}}_{en}^{\text{trial}})$ has been used.
 440 Finally, setting $\mathbf{s}_n = \|\mathbf{s}_n\| \mathbf{n}_n$ and $\mathbf{s}_n^{\text{trial}} = \|\mathbf{s}_n^{\text{trial}}\| \mathbf{n}_n^{\text{trial}}$, equation (44) can be rewritten as
 441 [15]

$$\left[\|\mathbf{s}_n\| + \frac{2}{3} \mu \gamma_{\tau n} \Delta t_n \text{tr}(\mathbf{g}\bar{\mathbf{b}}_{en}^{\text{trial}}) \right] \mathbf{n}_n = \|\mathbf{s}_n^{\text{trial}}\| \mathbf{n}_n^{\text{trial}}. \quad (45)$$

442 Since the sum in brackets on the left-hand-side of (45) is a non-negative scalar, the tensors
 443 \mathbf{n}_n and $\mathbf{n}_n^{\text{trial}}$ are parallel to each other, and, since they also have the same norm, it must
 444 hold that $\mathbf{n}_n = \mathbf{n}_n^{\text{trial}}$. Therefore, equation (45) also implies the equalities

$$\mathbf{s}_n = \mathbf{s}_n^{\text{trial}} - \frac{2}{3} \mu \gamma_{\tau n} \Delta t_n \text{tr}(\mathbf{g}\bar{\mathbf{b}}_{en}^{\text{trial}}) \mathbf{n}_n^{\text{trial}}, \quad (46a)$$

$$\|\mathbf{s}_n\| = \|\mathbf{s}_n^{\text{trial}}\| - \frac{2}{3} \mu \gamma_{\tau n} \Delta t_n \text{tr}(\mathbf{g}\bar{\mathbf{b}}_{en}^{\text{trial}}). \quad (46b)$$

445 Equation (46a) is the time-discrete flow rule (43) written in terms of stress, while, through
 446 the introduction of the yield functions

$$f_{\tau n} := \|\mathbf{s}_n\| - \sqrt{\frac{2}{3}} \left(K(\alpha_n) + \tau_y \right), \quad (47a)$$

$$f_{\tau n}^{\text{trial}} := \|\mathbf{s}_n^{\text{trial}}\| - \sqrt{\frac{2}{3}} \left(K(\alpha_{n-1}) + \tau_y \right), \quad (47b)$$

447 equation (46b) can be rephrased as

$$f_{\tau n} = f_{\tau n}^{\text{trial}} - \frac{2}{3} \mu \gamma_{\tau n} \Delta t_n \text{tr}(\mathbf{g}\bar{\mathbf{b}}_{en}^{\text{trial}}) - \sqrt{\frac{2}{3}} \left(K(\alpha_n) - K(\alpha_{n-1}) \right). \quad (48)$$

448 Consequently, the condition that plastic flow occurs at time t_n , obtained by setting $f_{\tau n} = 0$,
 449 is transformed into an equation that defines $\gamma_{\tau n}$ implicitly [15]:

$$\frac{2}{3} \mu \gamma_{\tau n} \Delta t_n \text{tr}(\mathbf{g}\bar{\mathbf{b}}_{en}^{\text{trial}}) + \sqrt{\frac{2}{3}} \left(K \left(\alpha_{n-1} + \sqrt{\frac{2}{3}} \gamma_{\tau n} \Delta t_n \right) - K(\alpha_{n-1}) \right) = f_{\tau n}^{\text{trial}}. \quad (49)$$

450 In (49), $f_{\tau n}^{\text{trial}}$ is regarded as known, and the time-discrete version of (35c) has been used to
 451 express α_n as a function of α_{n-1} and $\gamma_{\tau n}$. When the condition $f_{\tau n}^{\text{trial}} \leq 0$ applies, $\gamma_{\tau n} = 0$.
 452 In the case of non-linear hardening, (49) is non-linear too, and is solved numerically (e.g.
 453 by means of the Newton method). For linear hardening, $\hat{\mathfrak{H}}_{\kappa}$ is quadratic in α , and one
 454 obtains [15]

$$\gamma_{\tau n} \Delta t_n = \begin{cases} \frac{f_{\tau n}^{\text{trial}}}{\frac{2}{3} \mu \text{tr}(\mathbf{g}\bar{\mathbf{b}}_{en}^{\text{trial}}) + \frac{2}{3} H}, & \text{if } f_{\tau n}^{\text{trial}} > 0, \\ 0, & \text{if } f_{\tau n}^{\text{trial}} \leq 0, \end{cases} \quad (50)$$

455 where H is a constant material parameter having the same units as μ and defined by

$$H = \frac{\partial K}{\partial \alpha}(\alpha) = \frac{\partial^2 \hat{\mathfrak{H}}_{\kappa}}{\partial \alpha^2}(\alpha). \quad (51)$$

456 Both (49) and (50) determine $\gamma_{\tau n}$ as a function of \mathbf{F}_n (or, equivalently, as a functional
 457 of χ_n). Moreover, once $\gamma_{\tau n}$ is computed, α_n is obtained by $\alpha_n = \alpha_{n-1} + \sqrt{\frac{2}{3}} \gamma_{\tau n} \Delta t_n$, which
 458 is the time-discrete version of (35c). This decouples (35c) from (35a) and (35b).

459 The most important consequence of the assumptions discussed in this section is that,
 460 since $\mathbf{n}_n = \mathbf{n}_n^{\text{trial}}$ and $\text{tr}(\mathbf{g}\bar{\mathbf{b}}_{en}) = \text{tr}(\mathbf{g}\bar{\mathbf{b}}_{en}^{\text{trial}}) = \text{tr}(\mathbf{B}_{p(n-1)}\mathbf{C}_n)$, and none of these quantities
 461 depends on \mathbf{B}_{pn} , the flow rule (43) allows to express \mathbf{B}_{pn} as a non-linear function of χ_n :

$$\mathbf{B}_{pn} = \hat{\mathbf{B}}_{pn}(\chi_n) := \mathbf{B}_{p(n-1)} - \frac{2}{3}\Delta t_n \gamma_{\tau n}(\chi_n) \text{tr}(\mathbf{B}_{p(n-1)}\mathbf{C}_n) \mathbf{F}_n^{-1} \mathbf{n}_n^{\text{trial}} \mathbf{F}_n^{-\text{T}}, \quad (52)$$

462 with $\gamma_{\tau n}(\chi_n) > 0$. Here, it holds that $\mathbf{C}_n = \mathbf{F}_n^{\text{T}} \mathbf{g} \mathbf{F}_n$.

463 5.2 Time-Discrete Setting

464 By performing a backward Euler method in time, the results obtained in section 5.1 allow
 465 to reformulate the problem ‘Pr1’ as follows:

466

467 Given the initial data $\mathbf{B}_{p0}(X)$ and $\alpha_0(X)$ for all $X \in \mathcal{B}$, and the Dirichlet-boundary
 468 condition $\chi_{bn}(X)$ for all $X \in \partial\mathcal{B}_D$, find $\chi_n \in (H^1(\mathcal{B}, \mathcal{S}))^3$, $\mathbf{B}_{pn} \in \mathbf{L}^2(\mathcal{B}, T\mathcal{B} \otimes T\mathcal{B})$ and
 469 $\alpha_n \in L^2(\mathcal{B}, \mathbb{R})$ such that $\chi_n = \chi_{bn}$, for all $n \geq 0$ and $X \in \partial\mathcal{B}_D$ and, for all $n \geq 1$,

$$\mathbf{B}_{pn} = \begin{cases} \mathbf{B}_{p(n-1)}, & \text{if } \gamma_{\tau n} = 0, \\ \hat{\mathbf{B}}_{pn}(\chi_n) = \mathbf{B}_{p(n-1)} - \hat{\mathcal{R}}_n(\chi_n), & \text{if } \gamma_{\tau n} > 0, \end{cases} \quad (53a)$$

$$\alpha_n = \begin{cases} \alpha_{n-1}, & \text{if } \gamma_{\tau n} = 0, \\ \alpha_{n-1} + \sqrt{\frac{2}{3}} \gamma_{\tau n}(\chi_n) \Delta t_n, & \text{if } \gamma_{\tau n} > 0, \end{cases} \quad (53b)$$

$$\mathcal{P}'(\chi_n, \tilde{\mathbf{u}}) = \begin{cases} \int_{\mathcal{B}} \hat{\mathbf{P}}(\chi_n, \mathbf{B}_{p(n-1)}) : \mathbf{g} \text{Grad} \tilde{\mathbf{u}} = 0, & \text{if } \gamma_{\tau n} = 0, \\ \int_{\mathcal{B}} \hat{\mathbf{P}}(\chi_n, \hat{\mathbf{B}}_{pn}(\chi_n)) : \mathbf{g} \text{Grad} \tilde{\mathbf{u}} = 0, & \text{if } \gamma_{\tau n} > 0, \end{cases} \quad (53c)$$

470 where (53c) has to hold for all $\tilde{\mathbf{u}} \in \tilde{\mathcal{H}}$, $\gamma_{\tau n}(\chi_n)$ is determined either by (49) or by (50),
 471 and $\hat{\mathcal{R}}_n(\chi_n)$ is defined as

$$\hat{\mathcal{R}}_n(\chi_n) = \frac{2}{3} \Delta t_n \gamma_{\tau n}(\chi_n) \text{tr}(\mathbf{B}_{p(n-1)}\mathbf{C}_n) \mathbf{F}_n^{-1} \mathbf{n}_n^{\text{trial}} \mathbf{F}_n^{-\text{T}}. \quad (54)$$

472 The functional $\mathcal{P}'(\chi_n, \tilde{\mathbf{u}})$ is non-linear in χ_n regardless of whether $\gamma_{\tau n}$ is zero or positive.
 473 This is because the first Piola-Kirchhoff stress tensor is a non-linear constitutive functional
 474 of χ_n within the framework of finite deformations. Thus, iterative procedures (e.g. Newton
 475 method) are required to solve (53c). Note that the formulation of the RMA summarised
 476 above, which leads to (52) and (54), is such that \mathbf{B}_{pn} can be expressed as an explicit
 477 function of χ_n . In other words, the time-discrete flow rule (52) can be rewritten as

$$\mathcal{G}_n(\chi_n, \mathbf{B}_{pn}) = \mathbf{B}_{pn} - \mathbf{B}_{p(n-1)} + \hat{\mathcal{R}}_n(\chi_n) = \mathbf{0}, \quad (55)$$

478 with \mathcal{G}_n being non-linear in χ_n and affine in \mathbf{B}_{pn} . Consequently, no linearisation of the
 479 flow rule with respect to \mathbf{B}_{pn} is necessary. However, this simplification cannot be done if
 480 the assumptions discussed in Section 5 (decoupling of the strain energy density function as
 481 in (39), and approximation of the flow rule as in (40)) cannot be invoked. For example, this
 482 can be the case described in ‘Pr2’, where no hypotheses are done on the right-hand-side
 483 of (38b). This motivates the study of problems of the same type as ‘Pr2’ by means of the
 484 Generalised Plasticity Algorithm (GPA) proposed in this paper.

485 By using numerical quadrature rules within Finite Element Methods, the equations (49),
 486 (53a), (53b) and (54), are evaluated at the integration points of every finite element of the
 487 spatial discretisation of the problem.

488 Although this work does use the assumption of isotropy, the proposed algorithm does
 489 not invoke an approximation of the flow rule. This has the repercussions that the plastic

490 variable \mathbf{B}_{pn} cannot be rewritten as a function of the deformation χ_n , and, consequently,
 491 the flow rule cannot be decoupled from the balance of momentum. Rather, \mathbf{B}_{pn} has to
 492 be regarded as an unknown having, at least in principle, the same ‘dignity’ as χ_n . If, on
 493 the one hand, this complicates the numerical treatment of the elastoplastic problem, on
 494 the other hand, it makes the computational algorithm more flexible and applicable also
 495 to those cases, which do not require that $\mathbf{n}_n^{\text{trial}}$ is equal to \mathbf{n}_n . The proposed method is
 496 presented in detail in section 6.

497 6 Discretisation and Linearisation of the Problem ‘Pr2’

498 The discrete, linearised version of the problem ‘Pr2’ (cf. (37)–(38b)) is constructed in
 499 three steps. Firstly, a backward Euler method is used for discretising the flow rule (38b).
 500 Secondly, the time-discrete version of (38) is put in a form suitable for Finite Element
 501 analysis. Thirdly, the Finite Element Method is employed for the discretisation in space.

502 6.1 The Generalised Plasticity Algorithm (GPA)

503 The time-discrete version of the problem ‘Pr2’ can be formulated as follows:

504 Find $\chi_n \in (H^1(\mathcal{B}, \mathcal{S}))^3$ and $\mathbf{B}_{pn} \in \mathbf{L}^2(\mathcal{B}, T\mathcal{B} \otimes T\mathcal{B})$ such that $\chi_n = \chi_{bn}$, for all $n \geq 0$ and
 $X \in \partial\mathcal{B}_D$ and, for all $n \geq 1$,

$$505 \quad \mathcal{P}(\chi_n, \mathbf{B}_{pn}, \tilde{\mathbf{u}}) := \int_{\mathcal{B}} \hat{\mathbf{P}}(\chi_n, \mathbf{B}_{pn}) : \mathbf{g}\text{Grad } \tilde{\mathbf{u}} = 0, \quad \forall \tilde{\mathbf{u}} \in \tilde{\mathcal{H}}, \quad (56a)$$

$$506 \quad \mathcal{G}(\chi_n, \mathbf{B}_{pn}) = \mathbf{B}_{pn} - \mathbf{B}_{p(n-1)} + \hat{\mathcal{R}}_n(\chi_n, \mathbf{B}_{pn}) = \mathbf{0}, \quad \mathbf{B}_p(X, 0) = \mathbf{B}_{p0}(X) \text{ in } \mathcal{B}. \quad (56b)$$

507 Equations (56) are generally highly non-linear and coupled with each other. To search for
 508 solutions, (56a) and (56b) are linearised at each time step in a two-stage fashion according
 509 to Newton’s method. At the k th and l th iteration, $\chi_{n,k}$ and $\mathbf{B}_{pn,l}$ are written as

$$\chi_{n,k} = \chi_{n,k-1} + \mathbf{h}_{n,k}, \quad \mathbf{B}_{pn,l} = \mathbf{B}_{pn,l-1} + \Phi_{n,l}, \quad k, l \geq 1, \quad (57)$$

510 where $\mathbf{h}_{n,k}$ and $\Phi_{n,l}$ are the increments associated with χ_n and \mathbf{B}_{pn} , respectively. Thus, one
 511 can regard the deformation gradient tensor as a functional of the motion and write $\mathbf{F}_{n,k} =$
 512 $\mathbf{F}(\chi_{n,k})$ and $\mathbf{F}_{n,k-1} = \mathbf{F}(\chi_{n,k-1})$ as well as $\mathbf{H}_{n,k} = D_\chi \mathbf{F}_{n,k-1}[\mathbf{h}_{n,k}]$, the latter being the
 513 Gâteaux-derivative of the functional \mathbf{F} with respect to the motion, evaluated at $\chi_{n,k-1}$,
 514 and computed along the increment $\mathbf{h}_{n,k}$. It follows that $D_\chi \mathbf{F}_{n,k-1}[\mathbf{h}_{n,k}] = \text{Grad } \mathbf{h}_{n,k}$.

515 To describe the linearisation procedure in detail, it is useful to introduce the notation

$$D_\chi \mathcal{P}(\chi_{n,k-1}, \mathbf{B}_{pn}, \tilde{\mathbf{u}})[\mathbf{h}_{n,k}] = \int_{\mathcal{B}} \mathbf{g}\text{Grad } \tilde{\mathbf{u}} : \mathbb{A}(\chi_{n,k-1}, \mathbf{B}_{pn}) : \mathbf{H}_{n,k}, \quad (58a)$$

$$D_{\mathbf{B}_p} \mathcal{P}(\chi_n, \mathbf{B}_{pn,l-1}, \tilde{\mathbf{u}})[\Phi_{n,l}] = \int_{\mathcal{B}} \mathbf{g}\text{Grad } \tilde{\mathbf{u}} : \mathbb{B}(\chi_n, \mathbf{B}_{pn,l-1}) : \Phi_{n,l}, \quad (58b)$$

$$D_{\mathbf{B}_p} \mathcal{G}(\chi_n, \mathbf{B}_{pn,l-1})[\Phi_{n,l}] = \mathbb{Y}(\chi_n, \mathbf{B}_{pn,l-1}) : \Phi_{n,l}, \quad (58c)$$

516 with

$$\mathbb{A}(\chi_{n,k-1}, \mathbf{B}_{pn}) : \mathbf{H}_{n,k} = D_\chi \hat{\mathbf{P}}(\chi_{n,k-1}, \mathbf{B}_{pn})[\mathbf{h}_{n,k}], \quad (59a)$$

$$\mathbb{B}(\chi_n, \mathbf{B}_{pn,l-1}) : \Phi_{n,l} = D_{\mathbf{B}_p} \hat{\mathbf{P}}(\chi_n, \mathbf{B}_{pn,l-1})[\Phi_{n,l}]. \quad (59b)$$

517 The fourth-order tensor \mathbb{A} is the algorithmic acoustic tensor. The expressions defining
 518 explicitly \mathbb{A} , \mathbb{B} and \mathbb{Y} depend strongly on the constitutive model and on the flow rule.

519 The first stage of the GPA consists of linearising (56a) and (56b) with respect to \mathbf{B}_p
 520 only. This defines two approximated expressions of \mathcal{P} and \mathcal{G} that read at the l th iteration

$$\Delta_{\mathcal{P}} := \mathcal{P}(\chi_n, \mathbf{B}_{pn,l-1}, \tilde{\mathbf{u}}) + D_{\mathbf{B}_p} \mathcal{P}(\chi_n, \mathbf{B}_{pn,l-1}, \tilde{\mathbf{u}})[\Phi_{n,l}], \quad (60a)$$

$$\Delta_{\mathcal{G}} := \mathcal{G}(\chi_n, \mathbf{B}_{pn,l-1}) + \mathbb{Y}(\chi_n, \mathbf{B}_{pn,l-1}) : \Phi_{n,l}. \quad (60b)$$

521 Note that $\Delta_{\mathcal{P}}$ and $\Delta_{\mathcal{G}}$ are, respectively, a scalar and a second-order tensor since they are
 522 obtained by linearising the internal virtual power and the flow rule.

523 The dependence of \mathcal{G} on \mathbf{B}_{pn} (cf. (56b)) is such that \mathbb{Y} is invertible. Therefore, the
 524 increment $\Phi_{n,l}$ can be expressed as a function of χ_n by setting (60b) equal to zero, i.e.

$$\Phi_{n,l} = -[\mathbb{Y}(\chi_n, \mathbf{B}_{pn,l-1})]^{-1} : \mathcal{G}(\chi_n, \mathbf{B}_{pn,l-1}). \quad (61)$$

525 By substituting the right-hand-side of (61) into (60a), $\Phi_{n,l}$ is eliminated statically from
 526 $\Delta_{\mathcal{P}}$ (this is similar to an algorithm of Gauß-Seidel type), which becomes

$$\Delta_{\mathcal{P}} = \mathcal{P}(\chi_n, \mathbf{B}_{pn,l-1}, \tilde{\mathbf{u}}) - D_{\mathbf{B}_p} \mathcal{P}(\chi_n, \mathbf{B}_{pn,l-1}, \tilde{\mathbf{u}}) [[\mathbb{Y}(\chi_n, \mathbf{B}_{pn,l-1})]^{-1} : \mathcal{G}(\chi_n, \mathbf{B}_{pn,l-1})]. \quad (62)$$

527 At each time step, the motion χ_n is required to solve the equation $\Delta_{\mathcal{P}} = 0$. However,
 528 $\Delta_{\mathcal{P}}$ is defined in (62) as a highly non-linear functional of χ_n , $\Delta_{\mathcal{P}} \equiv \Delta_{\mathcal{P}}(\chi_n, \mathbf{B}_{pn,l-1}, \tilde{\mathbf{u}})$.
 529 The second stage of the GPA consists, thus, of linearising $\Delta_{\mathcal{P}}$ with respect to χ_n , and
 530 setting equal to zero its linearised expression. At the k th iteration of this linearisation
 531 sub-procedure, one has to solve

$$\Delta_{\mathcal{P}}(\chi_{n,k-1}, \mathbf{B}_{pn,l-1}, \tilde{\mathbf{u}}) + D_{\chi} \Delta_{\mathcal{P}}(\chi_{n,k-1}, \mathbf{B}_{pn,l-1}, \tilde{\mathbf{u}})[\mathbf{h}_{n,k}] = 0. \quad (63)$$

532 By introducing the auxiliary functional

$$g(\chi_n, \mathbf{B}_{pn,l-1}, \tilde{\mathbf{u}}) := D_{\mathbf{B}_p} \mathcal{P}(\chi_n, \mathbf{B}_{pn,l-1}, \tilde{\mathbf{u}}) [[\mathbb{Y}(\chi_n, \mathbf{B}_{pn,l-1})]^{-1} : \mathcal{G}(\chi_n, \mathbf{B}_{pn,l-1})], \quad (64)$$

533 $\Delta_{\mathcal{P}}$ becomes

$$\Delta_{\mathcal{P}}(\chi_n, \mathbf{B}_{pn,l-1}, \tilde{\mathbf{u}}) = \mathcal{P}(\chi_n, \mathbf{B}_{pn,l-1}, \tilde{\mathbf{u}}) - g(\chi_n, \mathbf{B}_{pn,l-1}, \tilde{\mathbf{u}}), \quad (65)$$

534 and (63) can be rewritten as

$$\begin{aligned} & \Delta_{\mathcal{P}}(\chi_{n,k-1}, \mathbf{B}_{pn,l-1}, \tilde{\mathbf{u}}) \\ & + D_{\chi} \mathcal{P}(\chi_{n,k-1}, \mathbf{B}_{pn,l-1}, \tilde{\mathbf{u}})[\mathbf{h}_{n,k}] - D_{\chi} g(\chi_{n,k-1}, \mathbf{B}_{pn,l-1}, \tilde{\mathbf{u}})[\mathbf{h}_{n,k}] = 0. \end{aligned} \quad (66)$$

535 The Gâteaux-derivative of g can be expressed by means of a fourth-order tensor \mathbb{A}' such
 536 that

$$D_{\chi} g(\chi_{n,k-1}, \mathbf{B}_{pn,l-1}, \tilde{\mathbf{u}})[\mathbf{h}_{n,k}] = \int_{\mathcal{B}} \mathbf{g} \text{Grad} \tilde{\mathbf{u}} : \mathbb{A}'(\chi_{n,k-1}, \mathbf{B}_{pn,l-1}) : \mathbf{H}_{n,k}, \quad (67)$$

537 which, by using (58a), allows to reformulate (66) as follows

538 Find $\mathbf{h}_{n,k} \in (H_0^1(\mathcal{B}, TS))^3$ such that, for all $n \geq 1$ and $k \geq 1$,

539
$$\bar{c}(\mathbf{h}_{n,k}, \tilde{\mathbf{u}}) = \bar{g}(\tilde{\mathbf{u}}), \quad \forall \tilde{\mathbf{u}} \in (H_0^1(\mathcal{B}, TS))^3, \quad (68)$$

540

541 where

$$\bar{c}(\mathbf{h}_{n,k}, \tilde{\mathbf{u}}) := \int_{\mathcal{B}} \mathbf{g} \text{Grad} \tilde{\mathbf{u}} : \bar{\mathbb{A}}_{n,k-1,l-1} : \text{Grad} \mathbf{h}_{n,k}, \quad (69a)$$

$$\bar{\mathbb{A}}_{n,k-1,l-1} := \mathbb{A}_{n,k-1,l-1} - \mathbb{A}'_{n,k-1,l-1}, \quad (69b)$$

$$\begin{aligned} \bar{g}(\tilde{\mathbf{u}}) &:= -\mathcal{P}(\chi_{n,k-1}, \mathbf{B}_{pn,l-1}, \tilde{\mathbf{u}}) \\ &+ \int_{\mathcal{B}} \mathbf{g} \text{Grad} \tilde{\mathbf{u}} : \left(\mathbb{B}_{n,k-1,l-1} : \mathbb{Y}_{n,k-1,l-1}^{-1} \right) : \mathcal{G}_{n,k-1,l-1}, \end{aligned} \quad (69c)$$

542 and the notation $\mathbb{A}_{n,k-1,l-1} = \mathbb{A}(\chi_{n,k-1}, \mathbf{B}_{pn,l-1})$, $\mathbb{B}_{n,k-1,l-1} = \mathbb{B}(\chi_{n,k-1}, \mathbf{B}_{pn,l-1})$, and
 543 $\mathbb{Y}_{n,k-1,l-1} = \mathbb{Y}(\chi_{n,k-1}, \mathbf{B}_{pn,l-1})$ has been used. The increments $\mathbf{h}_{n,k}$ belong, for all n and
 544 for all k , to the same functional space as the test velocities, i.e. $\mathbf{h}_{n,k}$ must vanish on $\partial\mathcal{B}_D$
 545 since, at each iteration and each time, the motion must comply with χ_b .

546 The tangent operator $\bar{\mathbb{A}}_{n,k-1,l-1}$ has been calculated by determining the numerical
 547 derivative of the right-hand-side of the functional $\Delta_{\mathcal{P}}$ (cf. (65)) with respect to the motion
 548 χ_n . This is because the explicit expression of g in (64) is very cumbersome.

549 6.2 Fully Discrete Linearised Setting

550 Let then \mathcal{T} be a regular triangularisation of $\text{Cl}(\mathcal{B}) = \mathcal{B} \cup \partial\mathcal{B}$ —the closure of \mathcal{B} — in N^h
 551 non-overlapping elements $\{T_i\}_{i=1}^{N^h}$, where $h > 0$ is the grid characteristic length. Moreover,
 552 let $\mathbb{P}_m(T_i)$ be the space of polynomials of order m over T_i , for all $i = 1, \dots, N^h$. Hence,
 553 setting for ease of notation $\mathcal{V} \equiv (H_0^1(\mathcal{B}, \mathcal{S}))^3$, the following linear finite element space is
 554 introduced

$$\mathcal{V}_m^h := \{ \tilde{\mathbf{u}}^h \in \mathcal{V} : \tilde{\mathbf{u}}_{|T_i}^h \in (\mathbb{P}_m(T_i))^3, \forall T_i \in \mathcal{T}, \tilde{\mathbf{u}}_{|\partial\mathcal{B}_D}^h = \mathbf{0} \}, \quad (70)$$

555 where the notation $(\mathbb{P}_m(T_i))^3$ means that each component of the vector-valued function
 556 $\tilde{\mathbf{u}}_{|T_i}^h$, restriction of $\tilde{\mathbf{u}}^h$ to the element T_i , is a polynomial of degree m (in the following, m
 557 will be either 1 or 2). The space \mathcal{V}_m^h is spanned by the Lagrangian basis functions $\{\boldsymbol{\varphi}^q\}_{q=1}^M$,
 558 with $M = \dim(\mathcal{V}_m^h)$, so that the approximations of the test velocity $\tilde{\mathbf{u}}$ and of the increment
 559 $\mathbf{h}_{n,k}$ can be written, at each time t_n and at each Newton iteration step k , as

$$\tilde{\mathbf{u}}^h = \sum_{q=1}^M \tilde{u}^q \boldsymbol{\varphi}^q, \quad \mathbf{h}_{n,k}^h = \sum_{q=1}^M h_{n,k}^q \boldsymbol{\varphi}^q \in \mathcal{V}_m^h. \quad (71)$$

560 The approximation of $\chi_{n,k} \in \mathcal{H}$ is constructed as in (57). At each time t_n , the sequence
 561 $\{\chi_{n,k}^h\}_{k \in \mathbb{N}}$ is contained in the set $\mathcal{H}^h \subset \mathcal{H}$ defined by

$$\mathcal{H}^h := \{ \chi_n^h \in \mathcal{H} : \chi_n^h|_{\partial\mathcal{B}_D} = \chi_{bn}^h \}, \quad (72)$$

562 where χ_{bn}^h is the approximation of the boundary data χ_b at time t_n . The approximated
 563 motion $\chi_{n,k-1}^h$, used to determine the right-hand-side of (57), is written as

$$\chi_{n,k-1}^h = y_n^h + \mathbf{h}_{n,k-1}^h \quad (73)$$

564 with $\mathbf{h}_{n,k-1}^h \in \mathcal{V}_m^h$ and $y_n^h|_{\partial\mathcal{B}_D} = \chi_{bn}^h$. Finally, the finite element version of (68) becomes:

565 Find $\mathbf{h}_{n,k}^h \in \mathcal{V}_m^h$ such that, for all $n \geq 1$ and $k \geq 1$,

566
$$\bar{c}(\mathbf{h}_{n,k}^h, \boldsymbol{\varphi}^q) = \bar{g}(\boldsymbol{\varphi}^q), \quad \forall q = 1, \dots, M. \quad (74)$$

567 The integrals featuring in $\bar{c}(\cdot, \cdot)$ and $\bar{g}(\cdot)$ are approximated by numerical quadrature.

568 7 Numerical Tests and Results

569 Due to the high non-linearity of the considered problems, the load attributed via the
 570 Dirichlet boundary conditions is applied incrementally. This leads to better starting values
 571 for the Newton method in every incremental step. Moreover, a line search method is applied
 572 to ensure global convergence of the non-linear iterations.

573 7.1 Comparison with the RMA for a Shear-Compression Test

574 As a first benchmark for evaluating the implementation of the GPA, and comparing it
 575 with the RMA, the shear-compression test of a unit cube presented in [56] is investigated.
 576 The unit cube is made of a material that is assumed to exhibit perfect plastic behaviour,
 577 i.e. no hardening is considered. Thus, the energy densities $\hat{\psi}_\kappa$ and \hat{W}_κ differ from each
 578 other additively by a constant (cf. (14)), q vanishes identically (cf. (15c)), and the model
 579 is described by \hat{W}_κ (cf. (39)) and the yield function $f_\tau(\boldsymbol{\tau}_\kappa) = \|\text{dev}(\boldsymbol{\tau}_\kappa)\| - \sqrt{(2/3)}\tau_y$.
 580 Moreover, since $q = -K(\alpha) = 0$, equation (49) delivers

$$\gamma_{\tau n} \Delta t_n = \begin{cases} \frac{f_{\tau n}^{\text{trial}}}{\frac{2}{3}\mu_{\text{tr}}(\mathbf{g}\mathbf{b}_{\text{en}}^{\text{trial}})}, & \text{if } f_{\tau n}^{\text{trial}} > 0, \\ 0, & \text{if } f_{\tau n}^{\text{trial}} \leq 0. \end{cases} \quad (75)$$

581 In an orthonormal Cartesian reference frame, the Dirichlet boundary conditions can be
 582 written as follows: For all $t \in \mathcal{J} \equiv [0, T]$,

$$\chi_b^1(X, t) = X^1 + 0.3\frac{t}{T}, \quad \chi_b^2(X, t) = X^2 - 0.3\frac{t}{T}, \quad \chi_b^3(X, t) = X^3, \quad \text{on } [X^1, 1, X^3], \quad (76a)$$

$$\chi_b^1(X, t) = X^1, \quad \chi_b^2(X, t) = X^2, \quad \chi_b^3(X, t) = X^3, \quad \text{on } [X^1, 0, X^3], \quad (76b)$$

583 with $[X^1, 1, X^3] = [0, 1] \times \{1\} \times [0, 1]$, $[X^1, 0, X^3] = [0, 1] \times \{0\} \times [0, 1]$. The conditions (76)
 584 describe a cube clamped at the bottom surface, $X^2 = 0$, and undergoing shear and com-
 585 pression at the top surface $X^2 = 1$ with a deformation up to 30%. The material parameters
 586 used for this test are reported in Table 1 (even though hardening is not considered in this
 587 example, the material parameters H_∞ , H , and ω are reported in Table 1, since they shall
 588 be used in next benchmarks). Note that the parameters reported in Table 1 are taken from
 589 [15], and model the material behaviour of steel (cf. [6]).

Table 1: Material parameters

bulk modulus	κ	164206.00 N/mm ²
shear modulus	μ	80193.80 N/mm ²
initial yield stress	τ_y	450.00 N/mm ²
saturation stress	H_∞	715.00 N/mm ²
linear hardening modulus	H	129.24 N/mm ²
hardening exponent	ω	16.93

590 To check whether the GPA (cf. Section 6.1) produces results comparable with the RMA,
 591 the maximal eigenvalue of the Kirchhoff stress tensor $\boldsymbol{\tau}_\kappa$ at the midpoint of the unit cube
 592 is computed (see Fig. 1). Both the RMA and the GPA determine the same results. In
 593 Figure 1, the deformation of the cube in the shear-compression test is shown at time
 594 $t = T = 300$ s. Moreover, in Table 2, the computed values of the invariants of the Mandel
 595 stress tensor $\boldsymbol{\Sigma}$ are reported for different deformations.

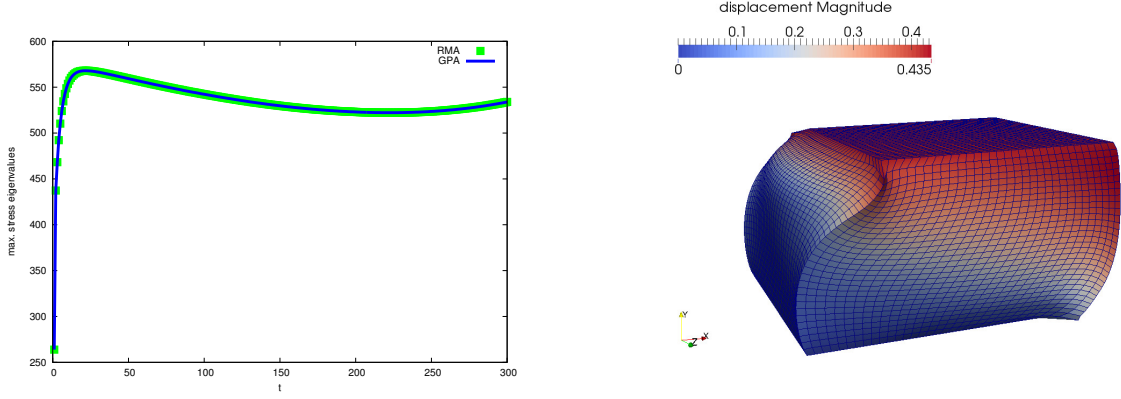


Figure 1: (Left) Maximal eigenvalue of τ_n at $X = (0.5, 0.5, 0.5)$ using the ‘RMA’ (green) and the ‘GPA’ (blue) with $T = 300$ s. (Right) Deformation of the unit cube in a shear compression test at $t = T = 300$ s.

Table 2: Comparison of the invariants of the Mandel stress tensor at $t = T/300$, $t = T/3$ and $t = T$, which correspond to deformations of 0.1%, 10% and 30%, respectively. The models M1, M2, M3, M4, M5 can be found in [56]. In the present paper, computations have been run with a modified version of model M4, which is referred to $\widetilde{M4}$ hereafter, while the results shown in [56] are taken as reference for comparisons. $\widetilde{M4}$ combines the energy potential of the model M4 [56], with the flow rule (40). The deformation at $t = T/300$ serves to check for non-linear elasticity, since no plastic strains occur.

	M1(10%)	M1(30%)	M2(10%)	M2(30%)	$\widetilde{M4}$ (10%)	$\widetilde{M4}$ (30%)
$\bar{I}_1(\Sigma)$	-9.485+02	-9.977+02	-9.251+02	-9.190+02	-9.218+02	-9.141+02
$\bar{I}_2(\Sigma)$	1.984+05	2.257+05	1.840+05	1.803+05	1.826+05	1.786+05
$\bar{I}_3(\Sigma)$	-1.161+07	-1.473+07	-1.013+07	-9.936+06	-1.002+07	-9.944+06
	M2(0.1%)	M3(0.1%)	M4(0.1%)	M5(0.1%)	$\widetilde{M4}$ (0.1%)	
$\bar{I}_1(\Sigma)$	-2.557+02	-2.550+02	-2.560+02	-2.563+02	-2.560+02	
$\bar{I}_2(\Sigma)$	-2.205+03	-2.253+03	-2.207+03	-2.210+03	-2.213+03	
$\bar{I}_3(\Sigma)$	3.228+04	3.201+04	3.232+04	3.235+04	3.232+04	

596 7.1.1 Structural Set-Up

597 *RMA*: Let $\mathbf{P}_n = \hat{\mathbf{P}}(\chi_n, \mathbf{B}_{pn})$ be the stress response defined by computing \mathbf{B}_{pn} as prescribed
598 by (52) and substituting the result into the time-discrete version of the constitutive expres-
599 sion of \mathbf{P} (37). As stated in Section 5.2, $\mathcal{P}'(\chi_n, \tilde{\mathbf{u}})$ is non-linear in χ_n . Therefore, an iterative
600 scheme has to be applied to determine χ_n at each time step. Let then $\chi_{n,k} = \chi_{n,k-1} + \mathbf{h}_{n,k}$,
601 $k \geq 1$, be the motion at the k th Newton iteration, where the increment $\mathbf{h}_{n,k}$ solves the
602 linearised equation

$$\mathcal{P}'(\chi_{n,k-1}, \tilde{\mathbf{u}}) + D_\chi \mathcal{P}'(\chi_{n,k-1}, \tilde{\mathbf{u}})[\mathbf{h}_{n,k}] = 0. \quad (77)$$

603 In the computations performed in this paper, the Gâteaux-derivative $D_\chi \mathcal{P}'(\chi_{n,k-1}, \tilde{\mathbf{u}})[\mathbf{h}_{n,k}]$
604 is approximated numerically. Then, the RMA is performed according to the scheme in
605 Algorithm 1.

606 *GPA*: The functionality of the GPA is outlined in Algorithm 2, where the notation

$$\mathcal{P}_{n,k,l} = \mathcal{P}(\chi_{n,k}, \mathbf{B}_{pn,l}, \tilde{\mathbf{u}}), \quad \mathcal{G}_{n,k,l} = \mathcal{G}(\chi_{n,k}, \mathbf{B}_{pn,l}), \quad (78a)$$

$$\mathbb{B}_{n,k,l} = \frac{\partial \hat{\mathbf{P}}}{\partial \mathbf{B}_p}(\chi_{n,k}, \mathbf{B}_{pn,l}), \quad \mathbb{Y}_{n,k,l} = \frac{\partial \mathcal{G}}{\partial \mathbf{B}_p}(\chi_{n,k}, \mathbf{B}_{pn,l}), \quad (78b)$$

607 has been used. As explained in Section 6.1, the index l enumerates, at each time step,
608 the iterations performed to linearise the equations with respect to \mathbf{B}_{pn} . At the l th iteration,
609 $\mathbf{B}_{pn,l}$ is computed as shown in (57), and the increment $\Phi_{n,l}$ is determined by (61).
610 To control the linearisation error introduced by this procedure, line 15 of Algorithm 2
611 is mandatory. As for the RMA, the Gâteaux-derivative in line 22 of Algorithm 2 is
612 approximated by computing the numerical derivative of the defect equation in line 8.
613

Algorithm 1 Solving the balance equation using the 'RMA'

```

1: if  $X \in \partial\mathcal{B}_D$  then
2:    $\mathbf{F}_{n,0} = T\chi_{bn}$ ;
3: else
4:    $\mathbf{F}_{n,0} = \mathbf{F}(\chi_{n-1}(X))$ ;
5: end if
6:  $k = 0$ ;
7:
8:  $(\mathbf{P}_{n,k}, \mathbf{B}_{pn}) = \text{RMA}(\mathbf{F}_{n,k}, \mathbf{B}_{p(n-1)})$ ;
9:
10:  $r_{n,k} := -\mathcal{P}'_{n,k} = -\int_{\mathcal{B}} \mathbf{P}_{n,k} : \mathbf{g}\text{Grad}\tilde{\mathbf{u}}$ ;
11:
12: if  $\|r_{n,k}\| \leq \epsilon_F$  then
13:    $(\mathbf{F}_n, \mathbf{B}_{pn}) = (\mathbf{F}_{n,k}, \mathbf{B}_{pn})$ ;
14: else
15:   determine  $\mathbf{h}_{n,k+1}$  by solving:
16:    $D_\chi \mathcal{P}'_{n,k}[\mathbf{h}_{n,k+1}] = r_{n,k}$ ;
17:
18:    $\mathbf{F}_{n,k+1} = \mathbf{F}_{n,k} + D_\chi \mathbf{F}_{n,k}[\mathbf{h}_{n,k+1}]$ ;
19:    $k = k + 1$ ;
20:   go to 8;
21: end if

```

Algorithm 2 Solving the balance equation using the 'GPA'

```

1: if  $X \in \partial\mathcal{B}_D$  then
2:    $\mathbf{F}_{n,0} = T\chi_{bn}$ ;
3: else
4:    $\mathbf{F}_{n,0} = \mathbf{F}(\chi_{n-1}(X))$ ;
5: end if
6:  $l = 0$ ;  $\mathbf{B}_{pn,0} = \mathbf{B}_{p(n-1)}$ ;
7:  $k = 0$ ;
8:  $r_{n,k,l} := -\mathcal{P}_{n,k,l} + \int_{\mathcal{B}} \mathbf{g}\text{Grad}\tilde{\mathbf{u}} : \mathbb{B}_{n,k,l}(\mathbb{Y}_{n,k,l})^{-1} : \mathcal{G}_{n,k,l}$ ;
9:
10: if  $\|r_{n,k,l}\| \leq \epsilon_F$  then
11:   compute  $\Phi_{n,l+1}$ :
12:    $\Phi_{n,l+1} = -(\mathbb{Y}_{n,k,l})^{-1} : \mathcal{G}_{n,k,l}$ ;
13:    $\mathbf{B}_{pn,l+1} = \mathbf{B}_{pn,l} + \Phi_{n,l+1}$ ;
14:
15:   if  $\|\mathcal{G}(\mathbf{F}_{n,k}, \mathbf{B}_{pn,l+1})\| \leq \epsilon_{B_p}$  then
16:      $(\mathbf{F}_n, \mathbf{B}_{pn}) = (\mathbf{F}_{n,k}, \mathbf{B}_{pn,l+1})$ ;
17:   else
18:      $l = l + 1$ ; go to 8;
19:   end if
20: else
21:   determine  $\mathbf{h}_{n,k+1}$  by solving:
22:    $D_\chi r_{n,k,l}[\mathbf{h}_{n,k+1}] = -r_{n,k,l}$ .
23:
24:    $\mathbf{F}_{n,k+1} = \mathbf{F}_{n,k} + D_\chi \mathbf{F}_{n,k}[\mathbf{h}_{n,k+1}]$ ;
25:    $k = k + 1$ ; go to 8;
26: end if

```

614 7.1.2 Computational Effort

615 Even for the simple case of a unit cube, a good mesh resolution is required to obtain
616 reliable results [56]. To this end, 32768 trilinear hexahedral elements have been used, which
617 lead to 262144 non-linear problems in \mathbb{R}^7 (indeed, the unknowns of the problems are six
618 independent components of \mathbf{B}_p and the Lagrange multiplier γ_τ , the latter being computed
619 with an 8-point Gauß quadrature rule) at every integration point for the defect evaluation
620 and the computation of the consistent tangent. ‘Level 4’ denotes the finest grid, which
621 consists of 32768 hexahedral elements, and is found by a threefold, uniform refinement of
622 the coarsest grid, ‘Level 1’, consisting of 64 hexahedral elements. The solving strategies
623 adopted in this paper are similar to those reported in [56]. The non-linear variational
624 problem in χ_n (which involves 107811 unknowns) is solved by applying the Newton method
625 and having recourse to numerical differentiation to approximate the tangent operators. The
626 linear sub-problems occurring within the Newton-iterations are solved by a preconditioned
627 Bi-CGSTAB method, in which the preconditioner is determined by means of a multigrid
628 cycle with a multigrid method. A Gauß-Seidel method served as smoother in the geometric
629 multigrid cycle. The non-linear convergence is ensured by means of a line-search method.

630 It is important to remark that, for the GPA, additional effort has to be taken into

631 account to compute the increments $\Phi_{n,l}$, which require the inversion of a fourth-order
632 tensor at every integration point. Therefore, the generalised algorithm developed in this
633 paper needs more computing time than the classical RMA (see Table 3). On the other
634 hand, this increase of computational time can be viewed as a measure of the “weight” of
635 the simplifying hypotheses (39) and (40) discussed in Section 5, right after equation (41).

Table 3: Computing time (in CPU-h) for using the RMA resp. the GPA in the shear-compression test.

	Level 1	Level 2	Level 3	Level 4
RMA	0.010	0.111	0.950	9.042
GPA	0.040	0.429	3.281	33.172

636 For the von Mises J_2 plasticity model presented in problem ‘Pr1’, only one iteration
637 step in l , cf. Algorithm 2, was necessary to achieve a prescribed tolerance of $\epsilon_{B_p} = 1 \cdot 10^{-8}$
638 in the computations performed in this paper.

639 7.2 Comparison with the RMA for the Necking of a Circular Bar

640 The sample has initial length $L_0 = 26.667$ mm and initial radius $R_0 = 6.413$ mm. In
641 cylindrical coordinates, $X = (R, \Theta, Z)$, $R \in [0, R_0]$, $\Theta \in [0, 2\pi)$, $Z \in [-L_0/2, L_0/2]$ denote,
642 respectively, the radial coordinate, the angle about the symmetry axis, and the axial
643 coordinate of the original geometry (initial configuration) of the specimen. The material
644 parameters are listed in Table 1. A description of this very well-documented problem can
645 be found, for example, in [15, 56, 66].

646 By exploiting the cylindrical symmetry of the bar, and assigning appropriate boundary
647 conditions, the computations can be performed on one eighth of the original geometry.
648 However, the computational grid in the necking region is refined to a greater degree than
649 in the rest of the specimen.

650 As suggested in [15], a non-linear hardening law is chosen. In particular, the hardening
651 potential is taken to be

$$\hat{\mathfrak{H}}_\kappa(\alpha) = \frac{1}{2}H\alpha^2 + (H_\infty - \tau_y)\alpha + (H_\infty - \tau_y)\frac{1}{\omega} [\exp(-\omega\alpha) - 1], \quad (79a)$$

$$q = -K(\alpha) = -\frac{\partial \hat{\mathfrak{H}}_\kappa}{\partial \alpha}(\alpha) = -[H\alpha + (H_\infty - \tau_y)(1 - \exp(-\omega\alpha))]. \quad (79b)$$

652 It should thus be necessary to apply a local Newton method to determine the plastic
653 multiplier $\gamma_{\tau n}$ in (49) in every global Newton iteration for χ_n . However, in order to reduce
654 the computational effort, and since $\gamma_{\tau n}$ can be viewed as a functional of χ_n through \mathbf{F}_n
655 (cf. (49)), $\gamma_{\tau n}$ is computed explicitly with respect to χ_n in every global Newton step.

656 The necking test is performed by applying to the specimen an axial displacement up to
657 $\chi_b^z(X, T) - Z = 7.0$ mm (which corresponds to an elongation of about 26% of the original
658 length), for all $X \in [0, R_0] \times [0, 2\pi) \times \{L_0/2\} \cup [0, R_0] \times [0, 2\pi) \times \{-L_0/2\}$, which constitutes
659 the Dirichlet-boundary. The final load is reached by several incremental loading steps.

660 7.2.1 Grid Refinement

661 The base-level, termed ‘Level 1’, consists of 120 hexahedral elements and the finer levels
662 are generated by regular refinement of the grid. For instance, Level 2 is similar to the grid
663 presented in [67].

664 To obtain results in good agreement with those reported in [15], a fine computational
665 grid with 61440 hexahedral elements was needed for the computations performed in this

666 paper. Such a fine grid was necessary to approximate adequately the physical behaviour
667 and the change of geometry of the specimen (cf. Figures 2(a) and 2(b)). One reason for
668 the necessity of such a refinement lies in the fact that volumetric locking effects, which
669 might arise as a consequence of the hypothesis of isochoric plastic flow, need to be avoided.
670 Another common approach to eliminate volumetric locking is to increase the polynomial
671 order of the finite element spaces [68, 69] instead of decreasing the mesh size. Figure 2(d)
672 shows that a good accuracy of the experimental data can already be obtained on grid level
673 2 by using quadratic finite element *ansatz* functions.

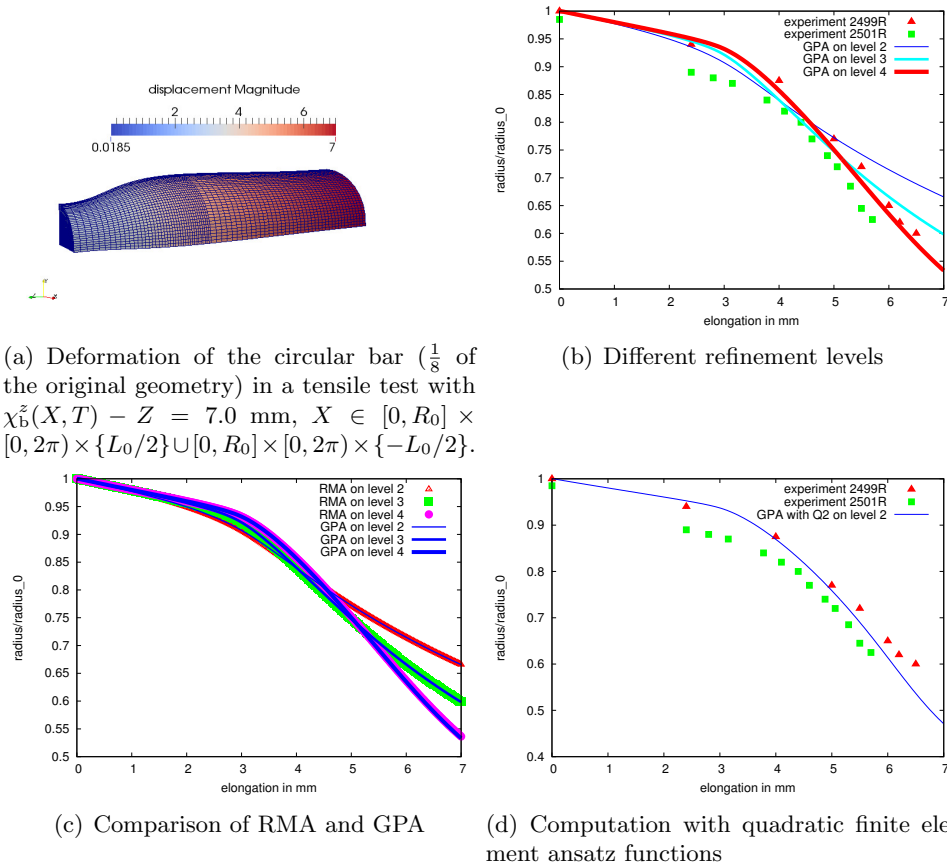


Figure 2: Comparison of the numerical results obtained in this work for the necking test to the experimental data reported in [70]. The experiments 2499R (21 °C) and 2501R (71 °C) differ from each other in the temperature of the specimen. The change of the sectional area where necking occurs is plotted against the elongation in mm.

674 7.2.2 Convergence

675 In Table 4, pointwise changes in the components of the displacement and in the normal
676 components of the Cauchy stress tensor $\sigma = J^{-1}PF^T$ are shown under uniform grid re-
677 finement. Although almost 200000 degrees of freedom are assigned on Level 4, the region
678 in which plastic evolution takes place is still not captured correctly (cf. Table 4). Never-
679 theless, linear convergence behaviour for the displacements and the normal stresses can
680 be observed at some representative sample points.

681 To discuss the convergence properties of the RMA and the GPA, it is necessary to look
682 at the Algorithms 1 and 2, and to recall that, in both cases, a non-linear problem in the
683 motion χ_n has to be solved at each time step. In particular, the RMA solves (53c), while
684 the GPA solves $\Delta_{\mathcal{P}} = 0$, where $\Delta_{\mathcal{P}}$ is given in (62). Due to the high non-linearity of the

Table 4: Let $P_1 = (6.413, 0, 13.334)$; $P_2 = (6.413, 0, 10)$; $P_3 = (6.406, 0.785, 12)$ be three sample points of the specimen expressed in cylindrical coordinates; $w^r := \chi^r(P, t) - \chi^r(P, 0)$ is the radial displacement and $w^z := \chi^z(P, t) - \chi^z(P, 0)$ is the longitudinal displacement at $P \in \{P_1, P_2, P_3\}$ and $t = 280$ s.

	elements	DoFs	plastic IPs	$w^r(P_1, t)$	diff.	$w^r(P_2, t)$	diff.	$w^z(P_3, t)$	diff.
Level 1	120	627	960	-1.548	0.590	-0.794	0.194	-1.815	0.997
Level 2	960	3843	4709	-2.138	0.423	-0.600	0.170	-2.812	0.469
Level 3	7680	26691	25539	-2.561	0.412	-0.530	0.009	-3.281	0.100
Level 4	70080	198531	110908	-2.973		-0.541		-3.381	
	$\sigma^{rr}(P_1, t)$	diff.	$\sigma^r(P_2, t)$	diff.	$\sigma^{zz}(P_3, t)$	diff.			
Level 1	3.646+03	1.099+03	5.734+03	2.297+03	3.860+03	8.277+03			
Level 2	2.547+03	0.489+03	8.031+03	4.558+03	12.137+03	3.475+03			
Level 3	2.058+03	0.316+03	3.473+03	0.687+03	8.662+03	0.710+03			
Level 4	1.742+03		2.786+03		7.952+03				

685 equations, iterative linearisation schemes are employed. These introduce *residuals* at each
686 iteration. For the RMA, the residual introduced at the k th iteration is denoted by $r_{n,k}$
687 (see line 10 of the Algorithm 1). For the GPA, the residual at the iterations k and l is
688 denoted by $r_{n,k,l}$ (see line 8 of the Algorithm 2). Both the iterative schemes used in this
689 paper converge, since the norm of the residual is smaller than, or equal to, a prescribed
690 tolerance (cf. line 12 of Algorithm 1 for the RMA, and line 10 of Algorithm 2 for the
691 GPA). It is also important, however, to establish how fast the iterative methods converge.
692 This can be done by counting the number of iteration steps required for satisfying the
693 conditions $\|r_{n,k}\| \leq \epsilon_F$ (line 12 of Algorithm 1) and $\|r_{n,k,l}\| \leq \epsilon_F$ (line 10 of Algorithm 2).
694 Looking at Table 5, it can be observed that the non-linear convergence rates of the RMA
695 and the GPA are comparable. For both algorithms, a line-search method is evident in the
696 first iteration steps for achieving convergence. Moreover, in both cases the convergence is
697 quadratic.

Table 5: Comparison of the non-linear reduction of the norm (absolute value, in the present context) of the residual as computed by the RMA and the GPA for the necking test on Level 4. The residual is the right-hand-side of line 10 of the Algorithm 1 for the RMA, and of line 8 of the Algorithm 2 for the GPA. The load applied at the Dirichlet boundary of the cylinder is $\chi_b^z(X, t) - Z = 7 \frac{t}{T}$ mm, with $T = 280$ s.

	RMA	$t = 1$ s	$t = 280$ s		GPA	$t = 1$ s	$t = 280$ s
nonlinear iteration step:	1	1.08+04	1.05+04	nonlinear iteration step:	1	1.07+04	1.05+04
	2	6.81+02	6.34+02		2	1.07+03	8.58+02
	3	5.51+02	5.48+02		3	3.20+02	8.24+02
	4	5.50+00	4.37+02		4	7.72+01	3.92+02
	5	5.26-02	2.70+02		5	7.63-01	6.44+01
	6	4.63-04	2.15+01		6	5.42-03	4.65+00
	7	2.86-06	1.01+01		7	3.91-05	1.48-01
	8	2.54-08	7.64-01		8	3.53-07	1.96-02
	9	3.53-10	5.99-02		9	2.39-09	6.04-04
	10		3.04-03		10		9.79-06
	11		4.11-05		11		8.67-08
	12		1.40-06		12		7.12-09
	13		1.55-08				
	14		6.58-09				

698 7.3 Shear-compression Test for a biomechanical example

699 To outline the wider field of application of the GPA in comparison to the classical RMA,
700 a biological flow rule of the form of (33) is chosen, i.e.

$$\dot{B}_p = -2\gamma_p B_p G \frac{\text{dev}(\Sigma_R)}{\|\text{dev}(\tau)\|}, \quad (80a)$$

$$\gamma_p := \lambda \left[\|\text{dev}(\tau)\| - \sqrt{(2/3)\tau_y} \right]_+. \quad (80b)$$

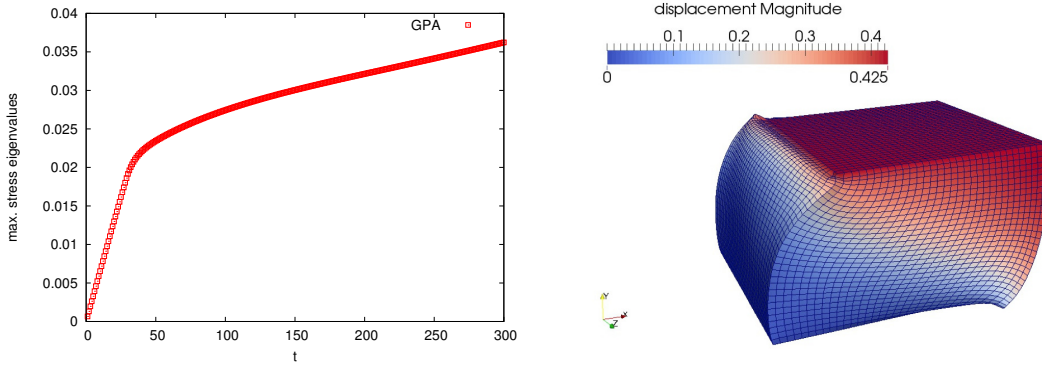


Figure 3: (Left) Maximal eigenvalue of $\boldsymbol{\tau}_\kappa$ at $X = (0.5, 0.5, 0.5)$ using the ‘GPA’ with $T = 300$ s. (Right) Deformation of the unit cube in a shear compression test for the biomechanical model at $t = T = 300$ s.

701 The mechanical response of the considered soft tissue, which is assumed to be hyperelastic,
 702 is modelled by means of the Holmes-Mow strain energy density function [71, 72, 73, 74]

$$\hat{W}_\kappa(\mathbf{C}_e) = \alpha_0 \left([\hat{I}_3(\mathbf{C}_e)]^{-\beta} \exp \left\{ \alpha_1 [\hat{I}_1(\mathbf{C}_e) - 3] + \alpha_2 [\hat{I}_2(\mathbf{C}_e) - 3] \right\} - 1 \right). \quad (81)$$

703 In (81), α_0 is a referential value of the strain energy density function, α_1 , α_2 and β are
 704 model parameters, while \hat{I}_1 , \hat{I}_2 and \hat{I}_3 are defined in (16a)–(16c). Clearly, \hat{W}_κ describes a
 705 material exhibiting isotropic elastic properties with respect to the natural state. As done
 706 in problem ‘Pr2’, \hat{W}_κ is a function of \mathbf{C}_e only. Moreover, hardening is disregarded here.

707 Since this model is based on the problem formulation ‘Pr2’, the application of the
 708 RMA in its classical form is not possible. Consequently, the GPA is validated for this
 709 biomechanical problem using the shear-compression test of the unit cube of section 7.1.
 710 The incremental load at the boundary is described by the Dirichlet boundary conditions
 711 (76). The material parameters used for this test are reported in Table 6. The elastic
 712 parameters α_0 , α_1 , and α_2 comply with the work of García and Cortés [72], who studied a
 713 model of articular cartilage. We selected β in such a way that $\beta = \alpha_1 + 2\alpha_2$ (cf. [71]). The
 714 material parameters incorporated in the phenomenological flow rule (80), which is suitable
 715 for biomechanical problems, are chosen in consistency with [58]. The computational grid
 716 consists of 32768 hexahedral elements.

Table 6: Material parameters

α_0 (N/mm ²)	α_1	α_2	β	λ	τ_y (N/mm ²)
0.722	0.150	0.024	0.198	0.500	0.020

717 The deformation of the cube in the shear-compression test is similar to that from
 718 Section 7.1 at time $t = T = 300$ s (cf. Figure 1 and Figure 3). However, the maximal
 719 eigenvalue of the Kirchhoff stress tensor $\boldsymbol{\tau}_\kappa$ at the midpoint of the unit cube differs from
 720 that found by the Neo-Hookean model (cf. Figure 1), and is plotted in Figure 3.

721 7.4 Software Framework UG4

722 The numerical methods presented in this work have been implemented in UG4, a novel
 723 version of the software framework UG (‘Unstructured Grids’) [75]. This toolbox provides
 724 fast, massive-parallel solvers for coupled partial differential equations like, e.g. geometric
 725 and algebraic multigrid methods. Its new tools for parallel communication (PCL) allow
 726 for an efficient scaling of the code on large numbers of processors [76].

727 8 Discussion and Outlook

728 As stated at the end of section 5.2, the algorithm proposed in this work treats \mathbf{B}_p and χ
 729 as equally ranked variables, even though technical reasons lead to a ‘hierarchical’ solution
 730 strategy, which suggests to compute first the plastic increment, $\Phi_{n,l}$, by solving (60b), and
 731 then to determine the increment of deformation, $\mathbf{h}_{n,k}$, by solving the problem (68). These
 732 reasons are also related to the fact that the weak form of the momentum balance law is
 733 solved by a Finite Element method, whereas the flow rule is defined pointwise and, as such,
 734 requires no spatial discretisation (rather, \mathbf{B}_p is evaluated only at the integration points of
 735 the finite elements). The philosophy of the algorithm has been inspired by the observation
 736 that the modelling choices proposed in [16, 17] comply with the development of some
 737 generalised numerical procedures (cf., e.g., [77]) that tend to improve the efficiency of the
 738 ‘standard’ algorithms of Computational Plasticity. In the authors’ opinion, this conceptual
 739 framework is suitable for a unified approach to the analysis of anelastic processes.

740 The theory reported in [16, 17] is based on the fundamental concept according to which
 741 a body that deforms and changes its internal structure is characterised by a “multi-layer
 742 kinematics” [17]. The kinematic descriptor associated with the “visible” motion of the
 743 body is the “standard velocity” \mathbf{v} (or \mathbf{u}), while the kinematic descriptor accounting for
 744 the variation of the body’s internal structure is the generalised velocity $\mathbf{L}_p = \dot{\mathbf{F}}_p \mathbf{F}_p^{-1}$ (or
 745 $\dot{\mathbf{B}}_p$). Consistently with the concept of “multi-layer kinematics”, the space of generalised
 746 virtual velocities is generally a subset of

$$\tilde{\mathcal{H}}_a := \{(\tilde{\mathbf{u}}, \tilde{\mathbf{L}}_p) \in TS \times (T\mathcal{C}_\kappa \otimes T^*\mathcal{C}_\kappa) \mid \tilde{\mathbf{u}}|_{\partial\mathcal{B}_D} = \mathbf{0}\}, \quad (82)$$

747 where the subscript ‘a’ indicates that $\tilde{\mathcal{H}}_a$ is obtained by augmenting $\tilde{\mathcal{H}}$ with $\tilde{\mathbf{L}}_p$ (cf. (6)).
 748 It is important to remark that, in this framework, \mathbf{F}_p is not an internal variable. This
 749 strong difference with the standard theory requires to reformulate the Principle of Virtual
 750 Powers. Indeed, a logical consequence of viewing $\tilde{\mathbf{L}}_p$ as a virtual velocity is that one has
 751 to introduce the external and internal forces, \mathbf{M}_{ext} and \mathbf{M}_{int} , power-conjugate with $\tilde{\mathbf{L}}_p$.
 752 Thus, if the material constitutive behaviour is of grade zero with respect to \mathbf{F}_p and of
 753 grade one in χ , one obtains

$$\mathcal{P}_{\text{ext}}(\tilde{\mathbf{u}}, \tilde{\mathbf{L}}_p) := \int_{\mathcal{B}} \mathbf{b}_R \cdot \tilde{\mathbf{u}} + \int_{\partial\mathcal{B}_N} \mathbf{f}_R \cdot \tilde{\mathbf{u}} + \int_{\mathcal{B}} \mathbf{M}_{\text{ext}} : \eta \tilde{\mathbf{L}}_p, \quad (83a)$$

$$\mathcal{P}_{\text{int}}(\tilde{\mathbf{u}}, \tilde{\mathbf{L}}_p) := \int_{\mathcal{B}} \mathbf{P} : \mathbf{g} \text{Grad} \tilde{\mathbf{u}} + \int_{\mathcal{B}} \mathbf{M}_{\text{int}} : \eta \tilde{\mathbf{L}}_p. \quad (83b)$$

754 By enforcing the PVP, i.e. setting $\tilde{\mathcal{P}}_{\text{int}}(\tilde{\mathbf{u}}, \tilde{\mathbf{L}}_p) = \tilde{\mathcal{P}}_{\text{ext}}(\tilde{\mathbf{u}}, \tilde{\mathbf{L}}_p)$ for all $(\tilde{\mathbf{u}}, \tilde{\mathbf{L}}_p) \in \tilde{\mathcal{H}}_a$, the
 755 local force balance $\mathbf{M}_{\text{int}} = \mathbf{M}_{\text{ext}}$ is obtained, in conjunction with the standard one given
 756 in (9a)–(9c). Moreover, in the case of isochoric plastic distortions, and in the absence of
 757 hardening, the plastic dissipation reads $(\mathbf{M}_{\text{int}} + \Sigma) : \eta \mathbf{L}_p \geq 0$, which suggests to express
 758 \mathbf{M}_{int} as the sum of a dissipative stress \mathbf{Y} and the negative of the Mandel stress tensor Σ ,
 759 so that $\mathbf{M}_{\text{int}} = \mathbf{Y} - \Sigma$. This result, together with the force balance $\mathbf{M}_{\text{int}} = \mathbf{M}_{\text{ext}}$, leads
 760 to $\mathbf{Y} = \mathbf{M}_{\text{ext}} + \Sigma$ [16, 17]. If, for simplicity, \mathbf{M}_{ext} is assumed to vanish, then the more
 761 stringent equality $\mathbf{Y} = \Sigma$ is obtained. The latter equality is consistent with the standard
 762 theory, where the plastic dissipation is identified with $\Sigma : \eta \mathbf{L}_p$.

763 In the case of vanishing external forces, the PVP can be rewritten as

$$\int_{\mathcal{B}} \mathbf{P} : \mathbf{g} \text{Grad} \tilde{\mathbf{u}} + \int_{\mathcal{B}} (\mathbf{Y} - \Sigma) : \eta \tilde{\mathbf{L}}_p = 0 \quad \forall (\tilde{\mathbf{u}}, \tilde{\mathbf{L}}_p) \in \tilde{\mathcal{H}}_a. \quad (84)$$

764 When \mathbf{Y} can be determined constitutively as a function \mathbf{L}_p [20, 36, 42, 43], the PVP (84)
 765 produces a system of coupled equations in the unknowns χ and \mathbf{F}_p . Since the equation

766 determining \mathbf{F}_p stems from the second summand of (84), which is not local, suitable
767 finite element basis functions for \mathbf{F}_p and $\tilde{\mathbf{L}}_p$ should be introduced, as it is done for χ
768 and $\tilde{\mathbf{u}}$. In particular, the algebraic form of the mixed problem (84), obtained after the
769 finite element discretisation and linearisation of (84), leads to a block matrix, in which the
770 extra-diagonal blocks couple the degree of freedom related to the standard deformation
771 with those related to the plastic distortions. The same conclusions could be drawn also
772 in the case of rate-independent plastic behaviour, by substituting the second term of (84)
773 with the weak form of some flow rule [77]. As a consequence of this approach, \mathbf{F}_p need not
774 be evaluated only at the integration points, as it happens in the standard theory.

775 If, on the one hand, the formulation (84) can be viewed as a reinterpretation of the
776 standard theory of Elastoplasticity, on the other hand, spatial discretisations for \mathbf{F}_p become
777 mandatory for those constitutive theories whose grade in \mathbf{F}_p is higher than the zeroth.
778 This could happen, for instance, within the theory of defects in elasto-plastic materials (cf.,
779 e.g., [78]). In this case, indeed, the Differential Geometry tools required by the theory, like
780 the Bilby-type connection $\left(\mathbf{A}^{(p)}\right)_{BD}^A = (\mathbf{F}_p^{-1})_{B\beta}^A \partial_{XD}(\mathbf{F}_p)_{\beta B}^B$, involve the differentiation
781 of \mathbf{F}_p with respect to material coordinates. In such situations, or even in those in which
782 the evolution law for \mathbf{F}_p is given by [79]

$$\dot{\mathbf{F}}_p = \mathbf{Z}(\mathbf{F}_p, \mathcal{R}_p, \text{Grad}\mathcal{R}_p, X), \quad (85)$$

783 where \mathcal{R}_p is the fourth-order curvature tensor associated with the plastic metric tensor
784 $\mathbf{C}_p = \mathbf{F}_p^T \boldsymbol{\eta} \mathbf{F}_p$, spatial discretisations for \mathbf{F}_p and $\tilde{\mathbf{L}}_p$ become necessary. In this respect, it
785 might be useful to consider computational algorithms like the one proposed in this paper.

786 For the reasons outlined so far, the GPA seems to be a promising algorithm for those
787 theories in which \mathbf{F}_p represents a structural degree of freedom, rather than an internal
788 variable. As it currently stands, the GPA is actually a step forward in this direction. In a
789 future work, the possibility of applying the GPA to such a two-field formulation of finite
790 strain Plasticity shall be investigated in the framework of Poroplasticity, and together with
791 the possibility of establishing robust solvers, whose efficiency has been already shown for
792 optimisation problems and for the Navier-Stokes equations by means of a simultaneous
793 solving process [80][81]. This could be an interesting approach for a further development
794 of efficient solvers for structural mechanical problems.

795 Finally, the GPA could be a useful computational tool for problems in which plasticity
796 is coupled with damage [82] as well as for biomechanical models of growth and tissue
797 adaptation involving higher order gradients of the deformation (see, e.g., [83, 84, 85, 86]),
798 for problems of remodelling of bone [87] and fibre-reinforced biological materials [88], and
799 also for studying problems involving the mechanical interaction between fluid and porous
800 matrix in compacting fluid-saturated grounds [89].

801 Acknowledgments

802 The Authors acknowledge the Goethe-Universität Frankfurt am Main (Germany), the
803 German Ministry for Economy and Technology (BMWi), contract 02E10326 [AG and
804 GW], the Baden-Württemberg-Stiftung [RP], and the Polytechnic of Turin, (Italy) [AG].

805 References

806 [1] Lubliner, J. *Plasticity Theory*. Dover Publications, Inc., Mineola, New York, 2008.

- 807 [2] Mićunović, MV. *Thermomechanics of viscoplasticity—fundamentals and applications*.
808 Gao, DY, Ogden, RW. (Eds.), *Advances in Mechanics and Mathematics*. Heidelberg:
809 Springer; 2009.
- 810 [3] Pinsky, PM, Ortiz, M, Pister, KS. Numerical integration of rate constitutive equations
811 in finite deformation analysis. *Comput Methods Appl Mech Engng* 1983; 40: 137–158.
- 812 [4] Pinsky, PM, Ortiz, M, Taylor, RL. Operator split methods in the numerical solution
813 of the finite deformation elastoplastic dynamic problem. *Comput Struct* 1983; 17(3):
814 345–359.
- 815 [5] Simo, JC, Ortiz, M. A unified approach to finite deformation elastoplasticity based
816 on the use of hyperelastic constitutive equations. *Comput Methods Appl Mech Engng*
817 1985; 49: 221–245.
- 818 [6] Simo, JC. *Numerical Analysis and Simulation of Plasticity*. Handbook of Numerical
819 Analysis, Vol. IV., Elsevier Science, 1998.
- 820 [7] Albery, J, Carstensen, C, Zarrabi, D. Adaptive numerical analysis in primal elasto-
821 plasticity with hardening. *Comput Methods Appl Mech Engng* 1999; 171: 175–204.
- 822 [8] Armero, F. Formulation of finite element implementation of multiplicative model
823 of coupled poro-plasticity at finite strains under fully saturated conditions. *Comput*
824 *Methods Appl Mech Engng* 1999; 171: 205–241.
- 825 [9] Han, W, Reddy, BD. *Plasticity – mathematical theory and numerical analysis*.
826 Springer, New York, 1999.
- 827 [10] Toupin, RA. Elastic materials with couple stresses. *Arch Ration Mech Anal* 1962,
828 11: 385–414.
- 829 [11] Mindlin, RD. Micro-structure in linear elasticity. *Arch Ration Mech Anal* 1964, 16:
830 51–78.
- 831 [12] Mindlin, RD. Second gradient of strain and surface tension in linear elasticity. *Int J*
832 *Solids Struct* 1965, 1: 417–438.
- 833 [13] Cleja-Tigoiu, S, Maugin, GA. Eshelby’s stress tensors in finite elastoplasticity. *Acta*
834 *Mech* 2000; 139: 231–249.
- 835 [14] Rice, JR. Inelastic constitutive relations for solids: an internal variable theory and
836 its application to model plasticity. *J Mech Phys Solids* 1971; 19: 433–455.
- 837 [15] Simo, JC, Hughes, TJR. *Computational Inelasticity*. New York, Springer; 1998.
- 838 [16] Cermelli, P, Fried, E, Sellers, S. Configurational stress, yield and flow in rate-
839 independent plasticity. *Proc R Soc A* 2001; A457: 1447–1467.
- 840 [17] DiCarlo, A, Quiligotti, S. Growth and balance. *Mech Res Commun* 2002; 29: 449–456.
- 841 [18] Mosler, J, Bruhns, OT. Towards variational constitutive updates for non-associative
842 plasticity models at finite strain: models based on a volumetric-deviatoric split. *Int*
843 *J Solids Struct* 2009; 46: 1676–1684.
- 844 [19] Rodriguez, EK, Hoger, A, McCulloch, AD. Stress-dependent finite growth in soft
845 elastic tissues. *J Biomech* 1994; 27: 455–467.

- 846 [20] Epstein, M, Maugin, GA. Thermomechanics of volumetric growth in uniform bodies.
847 *Int J Plasticity* 2000; 16: 951–978.
- 848 [21] Ambrosi, D, Mollica, F. On the mechanics of a growing tumor. *Int J Eng Sci*, 2002;
849 40: 1297–1316.
- 850 [22] Preziosi, L, Ambrosi, D, Verdier, C. An elasto-visco-plastic model of cell aggregates.
851 *J Theor Biol*, 2010; 262(1): 35–47.
- 852 [23] Rajagopal, KR. Multiple configurations in continuum mechanics. *Rep Inst Comput*
853 *Appl Mech* 1995; 6.
- 854 [24] Wieners, C. Nonlinear solution methods for infinitesimal perfect plasticity. *Z Angew*
855 *Math Mech* 2007; 87:643–660.
- 856 [25] Marsden, JE, Hughes, TJR. *Mathematical Foundations of Elasticity*. New York:
857 Dover Publications Inc.; 1983.
- 858 [26] Epstein, M. *The Geometric Language of Continuum Mechanics*. Cambridge: Cam-
859 bridge University Press; 2010.
- 860 [27] Kröner, E. Allgemeine Kontinuumstheorie der Versetzungen und Eigenspannungen.
861 *Arch Rational Mech Anal* 1959; 4: 273–334.
- 862 [28] Davini, C. Some remarks on the continuum theory of defects in solids. *Int J Solids*
863 *Struct* 2001; 38: 1169–1182.
- 864 [29] Preston, S, Elżanowski, M. Material uniformity and the concept of the stress space.
865 In: Bettina Albers (Ed.), *Continuous Media with Microstructure* (Collection in Honor
866 of Krzysztof Wilmański), pp. 91–101. Heidelberg: Springer; 2010.
- 867 [30] Maugin, GA, Epstein, M. Geometrical material structure of elastoplasticity. *Int J*
868 *Plasticity* 1998; 14: 90–115.
- 869 [31] Epstein, M, Elżanowski, M. *Material inhomogeneities and their evolution*. Berlin,
870 Springer; 2007.
- 871 [32] Flory, PJ. Thermodynamic relations for high elastic materials. *Trans Faraday Soc*
872 1961; 41:8 29–838.
- 873 [33] Ogden, RW. Nearly isochoric deformations: Application to rubberlike solids. *J Mech*
874 *Phys Solids* 1978; 26: 37–57.
- 875 [34] Lubarda, VA, Hoger, A. On the mechanics of solids with a growing mass. *Int J Sol*
876 *Struct* 2002; 39: 4627–4664.
- 877 [35] Menzel, A. Modelling of anisotropic growth in biological tissues. A new approach and
878 computational aspects. *Biomech Model Mechanobiol* 2005; 3: 147–171.
- 879 [36] Ambrosi, D, Guana, F. Stress-Modulated Growth. *Math Mech Solids* 2007; 12: 319–
880 342.
- 881 [37] Liu, Y, Zhang, H, Zheng, Y, Zhang, S, Chen, B. A nonlinear finite element model for
882 the stress analysis of soft solids with a growing mass. *Int J Sol Struc* 2014; 51(17):
883 2964–2978.

- 884 [38] Loret, B, Simões, FMF. A framework for deformation, generalized diffusion, mass
885 transfer and growth in multi-species multi-phase biological tissues. *Eur J Mech A-*
886 *Solid* 2005; 24: 757–781.
- 887 [39] Ambrosi, D, Guillou, A, Di Martino, ES. Stress-modulated remodeling of a non-
888 homogeneous body. *Biomechan Model Mechanobiol* 2008; 7: 63–76.
- 889 [40] Grillo, A, Wittum, G, Giaquinta, G, Mićunović, MV. A multiscale analysis of growth
890 and diffusion dynamics in biological materials. *Int J Eng Sci* 2009; 47: 261–283.
- 891 [41] Grillo, A, Federico, S, Wittum, G, Imatani, S, Giaquinta, G, Mićunović, MV. Evolu-
892 tion of a fibre-reinforced growing mixture. *Nuovo Cimento C* 2009; 32(1): 97–119.
- 893 [42] Ambrosi, D, Preziosi, L, Vitale, G. The insight of mixtures theory for growth and
894 remodeling. *Z Angew Math Phys* 2010; 61: 177–191.
- 895 [43] Grillo, A, Federico, S, Wittum, G. Growth, mass transfer, and remodeling in fiber-
896 reinforced, multi-constituent materials. *Int J Nonlinear Mech* 2012; 47: 388–401.
- 897 [44] Sciarra, G, dell’Isola, F, Hutter, K. A solid-fluid mixture model allowing for solid
898 dilatation under external pressure. *Continuum Mechanics and Thermodynamics* 2001;
899 13(5): 287–306.
- 900 [45] Lubarda, VA. Constitutive theories based on the multiplicative decomposition of de-
901 formation gradient: Thermoelasticity, elastoplasticity, and biomechanics. *Appl Mech*
902 *Rev* 2004; 57(2): 95–108.
- 903 [46] Simo, JC. A framework for finite strain elastoplasticity based on maximum plastic
904 dissipation and the multiplicative decomposition: Part I. Continuum Formulation.
905 *Comput Mech Appl M* 1988; 66:199–219.
- 906 [47] Bonet, J, Wood, RD. *Nonlinear Continuum Mechanics for Finite Element Analysis*.
907 Cambridge, New York: Cambridge University Press; 2008.
- 908 [48] Epstein, M, Maugin, GA. The energy-momentum tensor and material uniformity in
909 finite elasticity. *Acta Mech* 1990; 83: 127–133.
- 910 [49] Maugin, GA. *Material Inhomogeneities in Elasticity*. London: Chapman&Hall; 1993.
- 911 [50] Epstein, M, Maugin, GA. On the geometrical material structure of anelasticity. *Acta*
912 *Mech* 1996; 115(1/4): 119–131.
- 913 [51] Cleja-Tigoiu, S. Yield criteria in anisotropic finite elasto-plasticity. *Arch. Mech* 2005;
914 57: 81–102.
- 915 [52] Cleja-Tigoiu, S, Iancu, L. Orientational Anisotropy and Plastic Spin in Finite Elasto-
916 Plasticity. *Int J Sol Struc* 2011; 48(6): 939–952.
- 917 [53] Cleja-Tigoiu, S, Iancu, L. Orientational anisotropy and strength-differential effect in
918 orthotropic elasto-plastic materials. *Int J Plasticity* 2013; 47: 80-110.
- 919 [54] Montáns, FJ, Bathe, K-J. Computational issues in large strain elasto-plasticity: an
920 algorithm for mixed hardening and plastic spin. *Int J Numer Meth Engng* 2005;
921 63:159–196.
- 922 [55] Gabriel, G, Bathe, K-J. Some Computational Issues in Large Strain Elasto-Plastic
923 Analysis. *Computers and Structures* 1995; 56(2/3):249–267.

- 924 [56] Neff, P, Wieners, C. Comparison of models for finite plasticity: A numerical study.
925 *Comput Visual Sci* 2003; 6:23–25.
- 926 [57] Mićunović, M. Thermodynamical and self-consistent approach to inelastic ferromag-
927 netic polycrystals. *Arch Mech* 2006; 58(4-5): 393–430.
- 928 [58] Givero, C, Preziosi, L. Modelling the compression and reorganization of cell aggre-
929 gates. *Math Med Biol* 2012; 29: 181–204.
- 930 [59] Salsa, S. *Partial Differential Equations in Action: From Modelling to Theory*. Milan;
931 Heidelberg; New York: Springer, 2008.
- 932 [60] Hofstetter, G, Taylor, RL. Non-Associative Drucker-Prager Plasticity at Finite
933 Strains. *Communications in Applied Numerical Methods* 1990; 6: 583–589.
- 934 [61] Quintanilla, R, Saccomandi, G. The Importance of the Compatibility of Nonlinear
935 Constitutive Theories with Their Linear Counterpart, *J Appl Mech* 2007; 74: 455–460.
- 936 [62] Federico, S. Volumetric-Distortional Decomposition of Deformation and Elasticity
937 Tensor. *Math Mech Solids* 2010; 15: 672–690.
- 938 [63] Federico, S. Covariant Formulation of the Tensor Algebra of Non-Linear Elasticity.
939 *Int J Nonlin Mech* 2012; 47: 273–284.
- 940 [64] Vergori, L, Destrade, M, McGarry, P, Ogden, RW. On anisotropic elasticity and
941 questions concerning its finite element implementation. *Comput Mech* 2013, 52: 1185–
942 1197.
- 943 [65] Federico, S, Grillo A, Imatani, S. The linear elasticity tensor of incompressible ma-
944 terials. *Math Mech Solids* 2015; 20(6): 643–662.
- 945 [66] Needleman, A. A numerical study of necking in circular cylindric bars. *J Mech Phys*
946 *Solids* 1972; 20:111-127.
- 947 [67] Simo, JC, Armero, F. Geometrically nonlinear enhanced strain mixed methods and
948 the method of incompatible modes. *Int J Numer Meth Engng* 1992; 33: 1413-1449.
- 949 [68] Düster, A, Rank, E. A p-version finite element approach for two- and three-
950 dimensional problems of the J_2 flow theory with non-linear isotropic hardening. *Int*
951 *J Numer Meth Engng* 2002; 53: 49–63.
- 952 [69] Heisserer, U, Hartmann, S, Düster, A, Yosibash, Z. On volumetric locking-free be-
953 haviour of p-version finite elements under finite deformations. *Commun Numer Meth*
954 *Engng* 2008; 24:1019-1032.
- 955 [70] Norris, DM, Moran, B, Scudder, JK, Quinones, DF. A computer simulation of the
956 tension test. *J Mech Phys Solids* 1978; 26:1–19.
- 957 [71] Holmes, MH, Mow, VC. The nonlinear characteristics of soft gels and hydrated
958 connective tissues in ultrafiltration. *J Biomech* 1990; 23(11): 1145–1156.
- 959 [72] García, JJ, Cortés, DH. A nonlinear biphasic viscohyperelastic model for articular
960 cartilage. *J Biomech* 2006; 39: 2991–2998.
- 961 [73] Federico, S, Grillo, A. Elasticity and permeability of porous fibre-reinforced materials
962 under large deformations. *Mechanics of Materials* 2012; 44: 58–71.

- 963 [74] Tomic, A, Grillo, A, Federico, S. Poroelastic materials reinforced by statistically
964 oriented fibres—numerical implementation and application to articular cartilage. *IMA*
965 *Journal of Applied Mathematics* 2014; DOI:10.1093/imamat/hxu039.
- 966 [75] Vogel, A, Reiter, S, Rupp, M, Nägel, A, Wittum, G. UG4 - A Novel Flexible Software
967 System for Simulating PDE Based Models on High Performance Computers. *Comput*
968 *Visual Sci* 2013; DOI: 10.1007/s00791-014-0232-9
- 969 [76] Reiter, S, Vogel, A, Heppner, I, Rupp, M, Wittum, G. A Massively Parallel Geometric
970 Multigrid Solver on Hierarchically Distributed Grids. *Comput Visual Sci* 2013; 16(4):
971 151–164.
- 972 [77] Eve, RA, Reddy, BD. The variational formulation and solution of problems of finite-
973 strain elastoplasticity based on the use of a dissipation function. *Int J Numer Meth*
974 *Engng* 1994; 37: 1673–1695.
- 975 [78] Cleja-Tigoiu, S. Elasto-plastic materials with lattice defects modeled by second order
976 deformations with non-zero curvature. *Int J Fract* 2010; 166: 61–75.
- 977 [79] Epstein, M. Self-driven continuous dislocations and growth. In: *Mechanics of Material*
978 *Forces*, Advances in Mechanics and Mathematics, Volume 11, Chapter 13, 129–148.
- 979 [80] Schulz, V, Wittum, G. Transforming smoothers for PDE constrained optimization
980 problems. *Comput Visual Sci* 2008; 11: 207–219.
- 981 [81] Wittum, G. On the convergence of multigrid methods with transforming smoothers,
982 theory with application to the Navier-Stokes equations. *Numer Math* 1989; 54: 543–
983 563.
- 984 [82] Contrafatto, L, Cuomo, M. A new thermodynamically consistent continuum model
985 for hardening plasticity coupled with damage. *Int J Sol Struct*, 2002; 37: 3935–3964.
- 986 [83] Lekszycki, T, dell’Isola, F. A mixture model with evolving mass densities for describ-
987 ing synthesis and resorption phenomena in bones reconstructed with bio-resorbable
988 materials. *Z Angew Math Mech* 2012; 92(6): 426–444.
- 989 [84] Madeo, A, Lekszycki, T, dell’Isola, F. A continuum model for the biomechanical
990 interactions between living tissue and bio-resorbable graft after bone reconstructive
991 surgery. *CR Mecanique* 2011; 339: 625–640.
- 992 [85] Madeo, A, dell’Isola, F, Darve, F. A continuum model for deformable, second gradient
993 porous media partially saturated with compressible fluids. *J Mech Phys Solids* 2013;
994 61(11): 2196–2211.
- 995 [86] dell’Isola, F, Seppecher, P, Madeo, A. How contact interactions may depend on
996 the shape of Cauchy cuts in N th gradient continua: approach “à la D’Alembert”.
997 *Zeitschrift für Angewandte Mathematik und Physik* 2012; 63(6): 1119–1141.
- 998 [87] Giorgio, I, Andreaus, U, Madeo, A. The influence of difference loads on the remodeling
999 process of a bone and bioresorbable material mixture with voids. *Continuum Mech*
1000 *Thermodyn* 2014; DOI: 10.1007/s00161-014-0397-y
- 1001 [88] Grillo, A., Wittum, G., Tomic, A., Federico, S. Remodelling in statistically ori-
1002 ented fibre-reinforced materials and biological tissues *Math Mech Solids* 2014; DOI:
1003 10.1177/1081286513515265

1004 [89] dell'Isola, F, Rosa, L, Woźniak, Cz. A micro-structured continuum modelling com-
1005 pacting fluid-saturated grounds: the effects of pore-size scale parameter. *Acta Me-*
1006 *chanica* 1998; 127(1-4): 165–182.